TRIGGERING NOX2 / ROS SIGNALING DURING

DISUSE-INDUCED SKELETAL MUSCLE ATROPHY

A Dissertation

by

JEFFREY MACK HORD

Submitted to the Office of Graduate and Professional Studies of
Texas A&M University
in partial fulfillment of the requirements for the degree of

DOCTOR OF PHILOSOPHY

Chair of Committee,	John M. Lawler
Committee Members,	Susan A. Bloomfield
	James D. Fluckey
	L. Rene Garcia
Head of Department,	Richard B. Kreider

December 2016

Major Subject: Kinesiology

ABSTRACT

Prolonged periods of reduced mechanical loading lead to physiological changes such as a reduction in muscle mass and strength. These morphological and functional changes are allowed to take place to regulate muscle mass, metabolic demand, and availability of the amino acid pool. Dysregulation of a number of cell signaling pathways have been proposed as triggers of unloading-induced atrophy including Ca^{2+}, growth factors (e.g., IGF-1), heat shock proteins, and reactive oxygen species (ROS). ROS are causal in key disuse atrophy signaling events such as sarcolemma dislocation of nNOSμ and activation of the atrophy-inducing transcription factor FoxO3a. Upregulation of the Nox2 isoform of NADPH oxidase has been implicated in the disuse-associated increase in ROS production. Evidence indicates that activation of angiotensin II type 1 receptor (AT1R) is an upstream event leading to Nox2 complex formation and activity.

In the current study, we used an AT1R blocker (losartan) to test the hypothesis that AT1R activation is an upstream signaling event driving Nox2 complex activity, nNOSμ dislocation, FoxO3a activation, and thus the slow-to-fast fiber type shift and atrophy in the unloaded soleus. Rats were divided into 4 groups: ambulatory control (CON), ambulatory + Losartan (40 mg/kg/day) (CONL), 7-days hindlimb unloaded (HU), and HU + Losartan (HUL). We report that administration of losartan attenuated unloading-induced phenotypic alterations in the soleus muscle, including the shift in fiber type and reductions in muscle fiber cross-sectional area (CSA). Losartan

administration ameliorated increased ROS levels and the upregulation and activity of Nox2 following unloading. Furthermore, AT1R blockade during unloading mitigated nNOSμ dislocation from the sarcolemma. In addition, losartan treatment during disuse offered significant protection against the increase in nuclear localized FoxO3a. We conclude that AT1R attenuates disuse atrophy by inhibiting Nox2 signaling, thereby lessening the extent of nNOSμ dislocation, and activation of the pro-atrophic transcription factor FoxO3a.

Our findings identify important downstream effects of AT1R activation during mechanical unloading-induced atrophy. Furthermore, these data provide support for the usage of the FDA-approved AT1R blocker, losartan, as a treatment to mitigate the effects of disuse atrophy that occur during instances such as prolonged bed rest, limb casting, and spaceflight.

DEDICATION

To my Dad who taught me what it means to have true grit.

To my Mom who taught me to find the humor in each and every day.

I wouldn't have made it where I am today without those traits.

Thank You!

ACKNOWLEDGEMENTS

Without the guidance, mentorship, assistance, and friendship from others, the work presented in this dissertation, as well as all of the other work I was involved in during my time as a graduate student, would not have been possible.

First of all, I would like to thank my research advisor and committee chair, Dr. John Lawler, and the rest of my committee, Dr. Sue Bloomfield, Dr. Rene Garcia, and Dr. Jim Fluckey, for their guidance and support over the past few years. I truly appreciate the time and input that each of you offered. Each time that I had a conversation with any one of you, I walked away having learned something. I value the insight you all have been able to provide. I also greatly appreciate the advice offered concerning my transition towards a post-doctoral position and beyond.

I would also like to thank Department of Health and Kinesiology staff and the Comparative Medicine Program staff for making our jobs easier. Honestly, I'm not sure how I would have made it through graduate school without their assistance.

Of course, I would be remiss if I did not thank the funding institutions that permitted the various research activities that I was involved in as a Ph.D. student: Sydney and J.L. Huffines Institute for Sports Medicine and Human Performance, American College of Sports Medicine (ACSM), Texas Chapter of ACSM, National Aeronautics and Space Administration (NASA), and the College of Education and Human Development at Texas A&M University.

In addition, thank you to Dr. Alice Young and Dr. Marianne Evola for the opportunity to work in a research lab and spurring my interest in biomedical research. Thank you to Dr. Mike Massett for serving as a mentor and for the overall interest that you have shown in my development as a graduate student, as well as the excellent advice you have offered for my future endeavors.

Thanks to my friends and colleagues. Nobody can go through this process alone, and we were able to share our experiences and attempt to guide each other in the 'right' direction. Specifically, I would like to thank many of my fellow lab members that I worked with in the Redox Biology and Cell Signaling Laboratory, including Yang Lee, Dr. Rachel Botchlett, Dr. Vinicius Guzzonni, Dr. J. Matthew Kuczmarski, Erika Garcia-Villatoro, Dinah Rodriguez, Sarah Little, Marcela Garcia, Katherine Farris, and Kristian Falcon. Not to mention all of the other graduate comrades, such as Dr. S.K. Kim, Dr. Josh Avila, Dr. Heather Vellers, Jessica Cardin, Dr. Kevin Shimkus, and Jackie Perticone.

Finally, I would like to extend thanks to those closest to me. To my Dad, Terry Hord, for showing me what hard work really is, for being an excellent role model, and for always offering support. To my Mom, Ida Haley, for providing humor and laughter, and of course, for always being there. To Dr. Meredith Luttrell, for being my partner in crime, and who just so happens to be the smartest and prettiest girl in any room. We've kept each other sane and supported each other through everything Ph.D.'ing threw at us. Couldn't have done any of this without the support that I received from each of you. Thank You!

TABLE OF CONTENTS

LIST OF FIGURES

Page

LIST OF TABLES

Page

CHAPTER I

INTRODUCTION

Loss of skeletal muscle mass results in muscular weakness, which negatively impacts quality of life. Skeletal muscle wasting occurs as a comorbidity to chronic diseases, as well as in response to prolonged periods of disuse. In the absence of disease, mechanical unloading or reduced loading, such as limb immobilization, bed rest, or exposure to microgravity, result in muscle atrophy. Although great strides have been made in recent years towards unraveling the molecular complexities involved in the atrophic process, the fundamental causes of altered skeletal muscle proteostasis remain uncertain.

Seeking further understanding of the mechanistic and metabolic pathways involved in disuse atrophy and approaches to reduce, delay, or prevent this effect is of great importance. However, the etiology of disuse atrophy is poorly understood.
In order to identify and/or develop therapeutic interventions to effectively mitigate disuse muscle atrophy requires knowledge of the signaling pathways involved in the regulation of protein synthesis and degradation in skeletal muscle cells. Accumulating evidence indicates that elevated production of reactive oxygen species (ROS) plays a critical role in altering the pathways involved in synthesis and degradation. Indeed, over the last quarter century, undeniable evidence indicates that increased ROS production contributes to disuse-induced skeletal muscle atrophy (Kondo *et al.*, 1991; Lawler *et al.*, 2003; Powers *et al.*, 2007).

In the following chapters, we will focus on disuse atrophy as well as the roles and regulation of increased ROS production promoting muscle wasting. Chapter II will provide an overview of protein synthesis and protein degradation mechanisms and pathways involved in disuse atrophy. In addition, we will introduce the various sources of ROS along with evidence that ROS production plays a critical role in the regulation of both synthesis and degradation pathways. Furthermore, we will provide evidence implicating altered neuronal nitric oxide synthase (nNOS) localization as a critical event during disuse atrophy, which appears to occur in response to elevated levels of ROS.

Chapter III is comprised of an original study investigating a potential upstream molecular signaling event driving the production of NADPH oxidase isoform 2 (Nox2)-derived ROS during disuse atrophy. We previously reported that the sarcolemma-localized Nox2 plays a contributory role to disuse atrophy incurred during rodent hindlimb unloading (Lawler *et al.*, 2014); however, very little is understood concerning the regulation of Nox2 as a source of ROS in skeletal muscle, let alone during disuse atrophy. Clues from a variety of tissue types implicate ligand activation of angiotensin II type I receptor (AT1R) as an upstream signaling event promoting activation of Nox2 (Cabello-Verrugio *et al.*, 2012a; Balakumar & Jagadeesh, 2014). However, whether AT1R activation leads to Nox2 activation during hindlimb unloading-induced atrophy is unknown. Therefore, we sought to elucidate the role of AT1R – Nox2 signaling in the rodent hindlimb unloading model of disuse.

A concluding chapter will provide a summary and conclusion of our findings. We will tie-in our novel observations from Chapter III with those discussed in Chapter

II. Finally, we will discuss the relevance of our pre-clinical research and potential integration into a clinical context.

CHAPTER II

LITERATURE REVIEW: ROS AND NNOS IN THE REGULATION OF DISUSE-INDUCED SKELETAL MUSCLE ATROPHY

2.1 Introduction

Skeletal muscle plays a significant role in our overall health, survival, and our quality of life. It comprises about 40% of the total body mass and is a vital component to basic biological functions such as metabolism, respiration, and locomotion. Characterized by its highly dynamic and adaptable nature, skeletal muscle contains the ability to respond to a variety of stressors to alter its size and function. For example, increasing the workload and mechanical load will result in skeletal muscle hypertrophy, whereas lessening or removing the load will result in muscle atrophy (Goldberg *et al.*, 1975). Skeletal muscle atrophy is also a response to chronic disease (i.e. cachexia, congestive heart failure, aging). The physiological impact of muscle atrophy is characterized by muscle weakness, fatigability, and increased mortality. Therefore, uncovering the critical molecules, proteins, and signaling cascades that regulate skeletal muscle atrophy is an active area of biological and physiological research. While the cell signaling underlying skeletal muscle atrophy across wasting phenomena remains mysterious, there has been encouraging progress in recent years.

The reduction of mechanical load or complete unloading of skeletal muscle is often termed ‘disuse’. Disuse-induced skeletal muscle atrophy results in physiological changes such as a reduction in muscle mass and strength. The extent of disuse-induced

skeletal muscle atrophy depends on several factors such as age, degree of mechanical unloading, and the function and fiber type composition of the affected muscle. As previously mentioned, skeletal muscle wasting also occurs as a comorbidity to chronic disease, and has been observed in pathologies such as cancer, congestive heart failure, diabetes, chronic obstructive pulmonary disease (COPD), severe burn injury, inflammatory bowel disease, etc. Muscle wasting in these pathologies is partly due to muscle disuse, but overriding effectors include oxidative stress, inflammatory signaling and cytokines. Whether atrophy is primarily due to disuse or as comorbidity with disease, there are common atrophic signaling events that stimulate reduction in muscle fiber cross-sectional area (CSA), decreased muscle protein content, and decreased mass. In addition, atrophy promotes a reduction in capillary density, architectural disruptions of the myofiber, phenotypic alterations in fiber type, reduction in force production, and eventual weakness that corresponds with easily fatigable muscles. Indeed, it is skeletal muscle weakness and fatigability that are the major factors impacting the impairment in the quality of life of affected individuals.

As mentioned above, prolonged periods of disuse due to bed rest, limb immobilization, denervation, or hindlimb unloading result in skeletal muscle atrophy. Concomitant with reduction in muscle mass, disuse-induced atrophy also results in a shift in fiber type from the slower oxidative phenotype to the faster glycolytic phenotype. Skeletal muscle atrophy is due to an imbalance between synthesis and breakdown of muscle protein. While the majority of the published studies have focused on protein degradation, the impact of decreased protein synthesis is critical to the

wasting process. Recent papers have emphasized cross-talk between protein degradation and protein synthesis, centered around an Akt – FoxO axis. The impact of disuse-induced protein degradation is a complex process, with new players and pathways having been identified in recent years. Major roles in the degradation process are taken on by the ubiquitin proteasome pathway (UPP), caspase-3 / calpains, and the autophagic-lysosomal pathway.

There is direct evidence that elevation of oxidative stress occurs during disuse, and may serve as a trigger to atrophic signaling by promoting muscle protein degradation and reducing muscle protein synthesis. However, the exact sequence of events from the onset of disuse to the increased production of reactive oxygen species (ROS) and subsequent atrophic signaling has not yet been established. In this review we will provide (1) an overview of the various experimental models of disuse-induced atrophy, followed by (2) an overview of synthesis and degradation mechanisms and pathways involved in disuse-induced atrophy. Then we will introduce the (3) evidence that ROS production plays a critical role during disuse-induced atrophy, followed by (4) the regulation of neuronal nitric oxide synthase (nNOS) localization and activity in response to disuse.

2.2 Models of Disuse

Disuse-induced atrophy has been investigated in several different models in both humans and rodents. Due to the invasiveness of procuring muscle samples from subjects, rodent models of disuse atrophy are often used to study the tissue adaptations, cellular mechanisms and signaling cascades involved in disuse atrophy. A variety of models of

disuse atrophy have been developed to mimic the various clinical atrophy-inducing events. For instance, the rodent model of limb immobilization is limb casting. Another common model of disuse is hindlimb unloading by way of rodent tail suspension, a common experimental model used to mimic the physiological response to prolonged periods of bed rest or spaceflight. In addition, animal models have been used to investigate the impact on skeletal muscle due to spinal cord injuries or denervation. A common model used to examine disuse of the respiratory muscles (e.g., diaphragm) is the mechanical ventilation rodent model.

While there are a number of animal models of disuse-induced skeletal muscle atrophy, human paradigms of disuse are often used for research purposes as well, despite the invasiveness. For example, human models of limb immobilization (i.e., casting or leg brace), prolonged bed rest, and unilateral lower limb suspension (ULLS; e.g., immobilizing one leg and walking with crutches or knee walker) are used to examine inactivity-induced atrophy in patients.

2.3 Mechanisms of Disuse-Induced Skeletal Muscle Atrophy

2.3.1 Decreased Protein Synthesis and Elevated Protein Degradation

To maintain a basal level of skeletal muscle mass, a balance between protein synthesis and protein degradation is necessary. In recent years, there has been a significant on-going debate regarding the roles of protein synthesis and degradation during disuse atrophy. This is partly due to the different models (humans vs. rodents) that have been used. In general, the major difference between human and rodent disuse models concerns the relative rate of atrophy, with atrophy occurring at a much faster rate

in rats than in humans (Phillips *et al.*, 2009), although muscle fiber-type plays a significant role. While most of the available data indicates that there is an initial drop in synthesis rates along with an increase in rates of degradation, there is a contrasting view that in humans, disuse atrophy occurs primarily in response to reduced synthesis rates (Phillips *et al.*, 2009). This is derived from human studies that have found a reduction in synthesis, while data regarding breakdown is inconsistent (Ferrando *et al.*, 1996; Urso *et al.*, 2006; Chen *et al.*, 2007; de Boer *et al.*, 2007; Glover *et al.*, 2010) and, in some instances, the methodology is deemed questionable or unreliable (Tesch *et al.*, 2008). Data inconsistencies are due in part to the difficulties associated with measuring rates of protein degradation in humans, with most of the data collected relying on the expression of genes associated with specific protein degradation pathways. Obviously, additional studies are warranted to determine if reductions in protein synthesis are the driving force of atrophy or if there is simply a lack of data from human disuse studies. For a glimpse into this on-going debate of decreased synthesis vs. increased degradation, refer to a recent Journal of Physiology *Crosstalk* series (Phillips & McGlory, 2014; Reid *et al.*, 2014).

Accumulating evidence indicates that disuse-induced skeletal muscle wasting is due to a combination of the reduction in the rate of protein synthesis and an elevation in protein degradation. For instance, in the hindlimb unloading model skeletal muscle protein synthesis rates were reduced within the first 5 hours of disuse (Thomason *et al.*, 1989), and within 48 hours the decreased synthesis rate levels off at a steady-state (Thomason *et al.*, 1989). Prolonged periods of disuse are known to lead to an increase in

protein degradation (Bodine *et al.*, 2001). However, rapid increases in proteolysis have been reported during mechanical unloading as well (Arbogast *et al.*, 2007; Schiaffino *et al.*, 2013). Together, those data indicate that the loss of skeletal muscle protein during disuse is most likely the outcome of declining synthesis rates and elevated degradation rates, with the latter playing the dominant role (Schiaffino *et al.*, 2013; Egerman & Glass, 2014).

The key degradation components that promote skeletal muscle wasting include ubiquitin proteasome pathway (UPP), caspase-3 / calpains, serine protease, and autophagy-lysosomal pathways (Powers *et al.*, 2007; Schiaffino *et al.*, 2013). Primary targets of degradation during disuse atrophy include myofibrillar proteins, although sarcoplasmic proteins are also degraded (Munoz *et al.*, 1993).

2.3.2 Disuse Atrophy Signaling Cascades

A variety of physiological stimuli trigger skeletal muscle atrophy. For example, atrophy that occurs as a comorbidity with chronic disease is considered to be caused by increased levels of pro-inflammatory cytokines, endotoxins, glucocorticosteroids, and tumor-derived factors (Schiaffino *et al.*, 2013; Egerman & Glass, 2014). On the other hand, disuse-induced skeletal muscle atrophy occurs through a reduction in mechanical tension (Kandarian & Stevenson, 2002) and elevated levels of oxidative stress (Powers *et al.*, 2007).

In part, skeletal muscle atrophy can occur as the result of blunting the anabolic insulin-like growth factor-1 (IGF-1) signaling pathway. Activation of IGF-1 requires signaling through the IGF receptor (IGFR) and the insulin receptor substrate-1 (IRS-1),

which leads to phosphorylation of phosphatidylinositol-3 kinase (PI3K). Active PI3K then phosphorylates phosphatidylinositol-4,5-bisphosphate to phosphatidylinositol-3,4,5-trisphosphate in the sarcolemma, creating a binding site for Akt. Activation of Akt leads to active phosphorylation of mammalian target of rapamycin complex 1 (mTORC1). mTORC1 regulates synthesis through phosphorylation and activation of p70S6K and downstream inhibition of eukaryotic translation initiation factor 4E-binding protein 1 (4E-BP1). Data from numerous studies support the role of the IGF-1 / PI3K / Akt / mTORC1 signaling cascade in the regulation of skeletal muscle hypertrophy and atrophy (Schiaffino *et al.*, 2013; Egerman & Glass, 2014). For example, IGF-1 resistance has been reported after 14 days of hindlimb unloading in skeletal muscle of rats (Allen *et al.*, 1997). However, injections of growth hormone and IGF-1 during unloading have limited effect, possibly due to up regulation of IGF-1 binding proteins (Wittwer *et al.*, 2002). In addition, activation of Akt / mTORC1 and the downstream effectors is repressed during hindlimb immobilization and hindlimb unloading (Hornberger *et al.*, 2001; You *et al.*, 2010; Kelleher *et al.*, 2013). A critical event in this signaling cascade is the activation of Akt, which is suggested to be a transition point between hypertrophy and atrophy (Schiaffino *et al.*, 2013; Egerman & Glass, 2014).

Degradation pathways in skeletal muscle include the ubiquitin proteasome pathway (UPP), calcium-dependent caspase-3 / calpains, serine protease, and the autophagy-lysosomal pathway (Powers *et al.*, 2007; Schiaffino *et al.*, 2013). Calpains are thought to initiate proteolysis via unzippering of the Z-disc (Ferreira *et al.*, 2009; Salazar *et al.*, 2010; Talbert *et al.*, 2013a) during periods of disuse, while the primary

degradation pathway is believed to be the UPP (Solomon & Goldberg, 1996; Taillandier *et al.*, 1996). Recently, autophagic-lysosomal proteins (Taillandier *et al.*, 1996; Talbert *et al.*, 2013b) have been cited as contributory to unloading-induced proteolysis.

As the major proteolytic pathway during disuse atrophy, the UPP serves to breakdown myofibrillar and sarcoplasmic proteins in muscle fibers. Distinct components of the UPP include the E1, E2, and E3 ubiquitin ligases. E1 ubiquitin ligases activate ubiquitin, the activated ubiquitin is transferred to the E2 conjugating ligase, and the E3 ubiquitin ligases regulate the transfer of the ubiquitin to the targeted protein. Two critical tissue-specific E3 ubiquitin ligases, MuRF1 and MAFbx/Atrogin-1, are upregulated in response to a variety of atrophy-inducing events. Bodine *et al.* (2001) found that in response to various models of disuse (i.e., hindlimb unloading, limb immobilization, and denervation), transcription of MuRF1 and MAFbx/Atrogin-1 were increased (Bodine *et al.*, 2001). Under resting conditions in skeletal muscle these genes are expressed at relatively low levels; however following reductions in mechanical load, expression of these genes is quickly induced. Expression of both MuRF1 and MAFbx/Atrogin-1 is rapidly elevated in numerous models of atrophy and suggested to significantly contribute to the initiation of atrophy (Bodine & Baehr, 2014).

2.3.3 FoxO and NF-κB Signaling

Expression of both MuRF1 and MAFbx/Atrogin-1 are regulated by a variety of transcription factors, including members of the forkhead box O transcription factor family (FoxO1 and FoxO3a), nuclear factor kappa B (NFκB) transcription factors (p50 and Bcl3), and the glucocorticoid receptor (GR) (Sandri *et al.*, 2004; Sacheck *et al.*,

2007; Waddell *et al.*, 2008; Wu *et al.*, 2011). During prolonged periods of disuse alterations in the activity of glucocorticoids has not been shown, thus elevated expression of MuRF1 and MAFbx/Atrogin-1 are not likely due to GR signaling (Watson *et al.*, 2012).

However, during various atrophy-inducing states, including disuse, elevated expression of FoxO1/3a has been observed (Lecker *et al.*, 2004; Sacheck *et al.*, 2007; Senf *et al.*, 2008) along with FoxO1/3a transcriptional regulation of MuRF1 and MAFbx/Atrogin-1 (Sandri *et al.*, 2004; Stitt *et al.*, 2004; Waddell *et al.*, 2008). Cytoplasmic dephosphorylation of FoxO proteins leads to nuclear translocation where they function as transcription factors acting to suppress growth and promote apoptosis (Ramaswamy *et al.*, 2002). FoxO activation can be regulated upstream by Akt, which can phosphorylate multiple sites on FoxO to prevent its nuclear translocation (Brunet *et al.*, 1999; Sandri *et al.*, 2004; Latres *et al.*, 2005). However, findings from human studies indicate there may be a dissociation between Akt signaling and synthesis / degradation, leaving the exact mechanism of FoxO1/3a regulation unclear (Marimuthu *et al.*, 2011).

As previously mentioned, NFκB-associated transcription factors (Bcl3 and p50) have been shown to upregulate MuRF1 and MAFbx/Atrogin-1 in response to mechanical unloading (Jackman *et al.*, 2013). In the unloaded rat soleus, a significant increase in the nuclear concentration of NFκB / Inhibitor of κ B (IκB) proteins p50, c-Rel, and Bcl3 was observed; however, activation of the canonical NFκB dimers p50-p65 were not found to be significantly activated (Hunter *et al.*, 2002). Kandarian's group found that p50 and Bcl3 serve as transcription factors for MuRF1 and MAFbx/Atrogin-1 during rodent

hindlimb unloading, and knock out of each transcription factor led to sparing of the muscle (Hunter & Kandarian, 2004).

Recent data from the Kumar and Kandarian research groups indicates that NFκB signaling during disuse may be regulated in part by activation of the fibroblast growth factor-inducible 14 (Fn14) receptor. Fn14 transcription and protein levels are induced in skeletal muscle during immobilization, hindlimb unloading, and following denervation (Mittal *et al.*, 2010; Wu *et al.*, 2011). In contrast, remobilization or resistance exercise both lead to a reduction in Fn14 transcription (Mittal *et al.*, 2010). Those data suggest a mechanosensitive role for Fn14 and its downstream NFκB signaling.

While FoxO1/3a and NFκB transcription factors have received much attention related to disuse-induced atrophy signaling, they are not the only mediators involved. Recent work by the Adams research group has unveiled two novel transcription factors upregulated with disuse: activating transcription factor 4 (ATF4) (Ebert *et al.*, 2012; Fox *et al.*, 2014) and the tumor suppressor p53 (Fox *et al.*, 2014). Using a mouse model, Ebert *et al.* (2012) knocked out the ATF4 gene, consequently preventing expression of the growth-arresting protein Gadd45a, and observed a muscle sparing effect following 3 days of limb immobilization but not 7 days of immobilization (Ebert *et al.*, 2012). In a follow-up study, their group reported increased expression of p53 with immobilization (Fox *et al.*, 2014). Muscle fiber atrophy even occurred in the absence of ATF4, while simultaneous forced expression of both factors exacerbated disuse atrophy (Fox *et al.*, 2014). Their data suggest that ATF4 and p53 signal through independent, yet additive, routes during skeletal muscle atrophy by stimulating p21 (Ebert *et al.*, 2012; Fox *et al.*,

2014). Interestingly, neither ATF4 nor p53 act as transcription factors for MuRF1 or MAFbx/Atrogin-1 (Ebert *et al.*, 2012; Fox *et al.*, 2014), indicating that their transcriptional regulation of atrophy is through alternative ubiquitin ligases or other mechanisms. These novel data support the notion that attenuation of muscle atrophy is likely accomplished in several phases, and that multiple transcription factors participate in the regulation of the atrophic process.

2.3.4 Novel Disuse-Induced E3 Ubiquitin Ligases

As indicated in the above paragraph, regulation of atrophy is not due to upregulation of a single transcription factor, nor upregulation of a single E3 ubiquitin ligase. In recent years, independent investigators have identified novel E3 ligases that are linked to regulation of skeletal muscle during catabolic states. For instance, expression of a HECT domain ubiquitin ligase referred to as Nedd4-1 was increased in skeletal muscle in response to denervation (Batt *et al.*, 2006) and hindlimb unloading (Koncarevic *et al.*, 2007). In addition, the muscle ubiquitin ligase of SCF complex in atrophy – 1 (MUSA1) is another recently discovered F-box E3 ubiquitin ligase. Overexpression of MUSA1 promoted muscle loss, whereas RNA interference led to sparing of muscle mass (Sartori *et al.*, 2013; Milan *et al.*, 2015).

Moreover, atrophic signaling that leads to FoxO1/3a activation has been linked to increased expression of the mitochondrial E3 ligase 1 (Mul1) (Lokireddy *et al.*, 2012). Mul1 participates in the promotion of mitochondrial fragmentation, depolarization, and mitophagy, all of which are associated with mitochondrial dysfunction (Lokireddy *et al.*, 2012).

Examination of the negative regulation of IGF-1 signaling has unveiled new E3 ubiquitin ligases: Cbl-b and mitsugumin 53 (MG53 or TRIM72). For instance, Cbl-b has been observed to negatively regulate IGF-1 signaling during prolonged periods of unloading (Nakao *et al.*, 2009). MG53 targets the insulin receptor for degradation and subsequently ubiquitinates IRS-1 in skeletal muscle from mice with metabolic syndrome (Song *et al.*, 2013).

These are just a few of the E3 ligases that have been connected or possibly have connections to disuse atrophy. Advances in techniques, antibodies, genetic models, epigenetics, etc. will further our understanding of the players and cascades involved in atrophy signaling.

2.4 Reactive Oxygen Species (ROS) Production in Skeletal Muscle During Disuse-Induced Atrophy

2.4.1 Oxidative Stress and Disuse-Induced Skeletal Muscle Atrophy

It has been 25 years since the first study connecting elevated levels of oxidative stress to disuse-induced skeletal muscle atrophy (Kondo *et al.*, 1991). Kondo et al. (1991) found that immobilization-induced atrophy in rats was associated with increased oxidative stress. Furthermore, the antioxidant properties of vitamin E attenuated the degree of atrophy (Kondo *et al.*, 1991). Since their novel findings were published, supporting data has accumulated suggesting the role/s of specific oxidant sources and antioxidants during the atrophic process. Furthermore, the manipulation of which can lead to muscle sparing effects during disuse (Lawler *et al.*, 2003; Min *et al.*, 2011; Lawler *et al.*, 2014). Altogether, the growth and progress of this field of interest has

driven the investigative efforts examining the roles of ROS, redox modifications, and associated signaling events that lead to skeletal muscle atrophy during prolonged periods of disuse.

2.4.2 ROS Production in Skeletal Muscles During Prolonged Periods of Disuse

Oxidative stress occurs when there is an imbalance between pro-oxidants and antioxidants, with the imbalance favoring the build-up of oxidized molecules within the cell or tissue (Lawler *et al.*, 2016). An ever-growing body of evidence indicates that disuse leads to elevated levels of oxidized proteins and lipids within skeletal muscle. Increased cellular concentrations of oxidized proteins and lipids, which are essentially damaged, are the result of elevated activities of pro-oxidant sources and ROS, as well as a reduction in the antioxidant capacity of the myofiber (Lawler *et al.*, 2016). To investigate this phenomenon, researchers have focused on the pro-oxidant sources within skeletal muscle fibers. Accumulating evidence suggests that skeletal muscle disuse leads to ROS production from various sources, including the mitochondria, xanthine oxidase (XO), and NADPH oxidase (Nox).

Strong evidence from mechanical ventilation and hindlimb immobilization studies indicates that a primary source of ROS during skeletal muscle disuse is the mitochondria (Min *et al.*, 2011; Talbert *et al.*, 2013b; Hudson *et al.*, 2015). For instance, mitochondrial release of hydrogen peroxide is increased more than 2-fold in the soleus and plantaris from rodents that endured 2 weeks of hindlimb immobilization (Min *et al.*, 2011). However, it is currently unknown if both populations of skeletal muscle

mitochondria, subsarcolemmal and intermyofibrillar, contribute to this elevation in ROS production.

In the series of pioneering work from Kondo *et al.* in the early 1990's, Kondo and colleagues suggested that XO may be the primary source of ROS in myofibers during disuse (Kondo *et al.*, 1993). Since then, however, data inconsistencies have been reported concerning XO and disuse. Evidence from mechanical ventilation experiments indicates that XO plays a significant role in oxidative injury and contractile dysfunction during periods of disuse (Whidden *et al.*, 2009). In agreement, XO inhibition blunted the severity of disuse-induced contractile dysfunction caused by hindlimb unloading, even though XO inhibition did not spare the soleus muscle from atrophy (Matuszczak *et al.*, 2004). In contrast, XO inhibition during hindlimb unloading has been found to offer significant muscle sparing effects (Derbre *et al.*, 2012). Altogether, the evidence implicates XO as having a regulatory role in the decline of contractile function associated with disuse, but it is still unclear whether or not XO promotes disuse atrophy.

Two Nox isoforms are expressed in skeletal muscle fibers, Nox2 (Semprun-Prieto *et al.*, 2011; Lawler *et al.*, 2014) and Nox4 (Sun *et al.*, 2011). The Nox2 isoform is a plasma membrane associated multi-subunit complex that is capable of actively producing superoxide when cytosolic subunits bind to the membrane-bound subunits. Sustained activation of Nox, in particular Nox2, has been associated with skeletal muscle atrophy *in vitro* and *in vivo* (Semprun-Prieto *et al.*, 2011; Abrigo *et al.*, 2016). Our group recently reported that 54 hours of hindlimb unloading was associated with increased sarcolemmal localization of two Nox2 subunits, gp91phox and p47phox

(Lawler *et al.*, 2014). Moreover, oxidative stress in response to mechanical ventilation has been linked to contractile dysfunction and fiber atrophy, both of which were attenuated by the administration of a Nox inhibitor (McClung *et al.*, 2009). The limited evidence indicates that disuse-induced oxidative stress is partially the result of Nox activation. Links between Nox2 and mitochondrial ROS are currently unknown in disuse atrophy.

2.4.3 Mechanistic Links Between Oxidative Stress and Disuse-Induced Atrophy

Oxidative stress has been linked to the manipulation and slowing of the rate of muscle protein synthesis. Accumulating evidence from *in vitro* experiments suggest that elevated ROS concentrations interfere with the phosphorylation of Akt/mTORC1 signaling and, in effect, limit translational efficiency (O'Loghlen *et al.*, 2006; Shenton *et al.*, 2006; Zhang *et al.*, 2009; Tan *et al.*, 2015). As previously mentioned, activation of Akt is suggested to be a transition point between hypertrophy and atrophy. Decreased Akt phosphorylation often results in lower rates of protein synthesis and increased degradation, which lead to atrophy. Recent *in vivo* investigations, have found that the disuse-associated increase in mitochondrial derived oxidants led to reductions in Akt activity (Talbert *et al.*, 2013b; Hudson *et al.*, 2015). For instance, elevated ROS in the immobilized soleus led to significant reductions in phosphorylation of Akt and mTORC1 (Talbert *et al.*, 2013b). Moreover, oxidative stress-associated inhibition of Akt, mTORC1, PRAS40, and 4E-BP1 were observed recently following mechanical ventilation (Hudson *et al.*, 2015). These findings indicate that disuse-induced oxidative

stress reduces protein synthesis by inhibiting Akt/mTORC1 signaling and limiting translation.

A growing body of evidence suggests that oxidative stress contributes to elevated rates of skeletal muscle proteolysis and atrophy through various routes. For instance, alterations in ROS production and signaling can regulate transcription factors and eventual gene expression of critical components of the UPP (Talbert *et al.*, 2013b; Lawler *et al.*, 2014). For example, disuse-associated oxidative stress has been shown to lead to increased dephosphorylation of cytoplasmic FoxO3a, which is suggestive of elevated nuclear FoxO3a content and activity (Lawler *et al.*, 2014). Moreover, increased ROS due to hindlimb immobilization has been shown to significantly increase expression of FoxO3a target genes: MuRF-1 and MAFbx/Atrogin-1 (Talbert *et al.*, 2013b). Furthermore, disuse-induced oxidative stress promotes increased activity of the 20S proteasome (Betters *et al.*, 2004).

Elevations in ROS production during disuse have also been implicated in regulating the expression and activity of components of the autophagy-lysosomal degradation pathway. For instance, inhibition of mitochondrial-derived ROS during disuse reportedly prevents the rise in autophagic vesicle formation and cathepsin expression (Talbert *et al.*, 2013b). Disuse-induced elevations in ROS production have also been linked to the activation of both calcium-mediated calpains and caspase-3 (Min *et al.*, 2011; Talbert *et al.*, 2013b). Additionally, elevated levels of disuse-induced ROS can promote proteolysis in muscle fibers by oxidizing proteins thereby enhancing their susceptibility to proteolytic degradation (Ikemoto *et al.*, 2002; Smuder *et al.*, 2010). For

example, antioxidant administration during hindlimb unloading effectively attenuates protein ubiquitination and fragmentation of myosin heavy chain proteins (Ikemoto *et al.*, 2002). Altogether, those data strongly suggest a significant role for oxidative stress in the regulation of disuse-induced proteolysis.

Possible links between disuse-associated ROS and NFκB, ATF4, p53, and several of the recently discovered atrogenes leave many unanswered questions in atrophy signaling. The limited data that is available points towards the likelihood that many of these transcription factors and atrogenes are altered in response to disuse-associated ROS. For example, antioxidant treatment during mechanical ventilation has verified oxidative stress as an upstream activator of NFκB and linked to diaphragm muscle weakness (Smuder *et al.*, 2012). Furthermore, ATF4 expression was highly responsive to hydrogen peroxide stimulation in C2C12 myotubes (Pierre *et al.*, 2014). In mechanically unloaded skeletal muscles, increased content of p53 has been suggested to lead to disturbances in the oxidative balance of the myofiber (Siu & Alway, 2005). Elevated levels of ROS have also been shown to induce expression of NEDD4-1 in brains from patients with Alzheimer's, Parkinson's, and Huntington's diseases and spinal cords from amyotrophic lateral sclerosis (ALS) patients (Kwak *et al.*, 2012). Additionally, recent evidence indicates that anthocynin (delphinidin) treatment during hindlimb unloading suppressed the expression of genes associated with oxidative stress while concomitantly preventing the rise in Cbl-b expression (Murata *et al.*, 2016). Accumulating evidence suggests that ROS exerts a strong influence on transcriptional

regulation during disuse atrophy, possibly beyond what is currently known. Refer to **Figure 2.1** for our proposed model of ROS regulation of atrophy gene transcription.

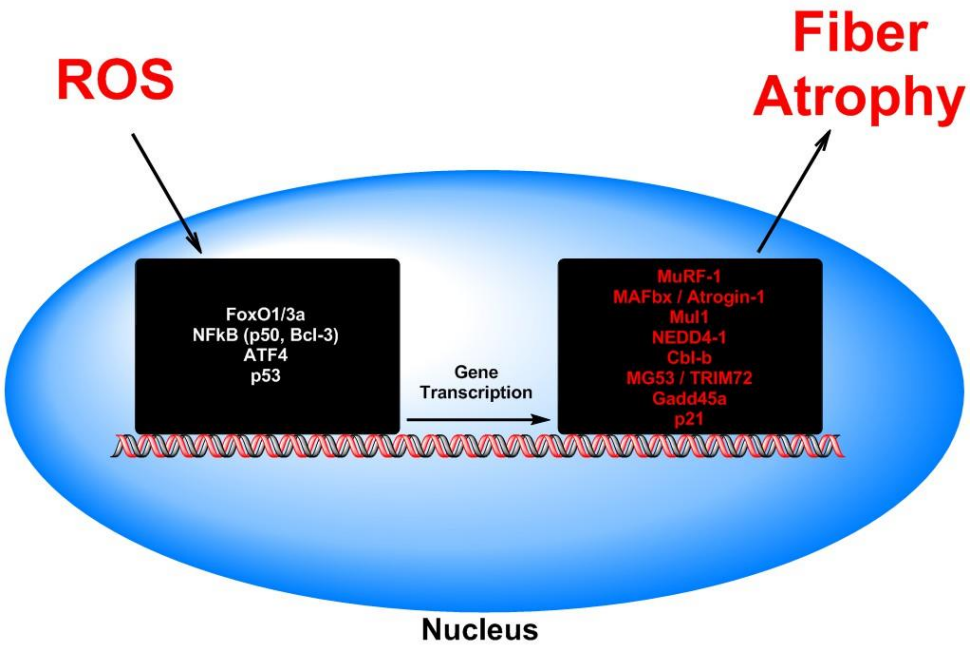

Figure 2.1. ROS regulation of transcription factors and expression of proteins involved in promoting the reduction of fiber size due to disuse. Based on published findings, we propose a list of transcription factors along with E3 ligases and growth arresting proteins known to directly promote atrophy or exert blunting effects on synthesis pathways, each of which is likely influenced by elevated myofiber ROS. This is a simplified figure illustrating ROS-regulation of disuse fiber atrophy; refer to text for further discussion. Transcription factors listed do not necessarily correspond to the list of E3 ligases and growth arresting factors.

Altogether, a growing body of evidence suggests that oxidative stress can impede the rate of protein synthesis and accelerate protein degradation in a variety of ways, resulting in skeletal muscle atrophy. However, several gaps in knowledge are evident

concerning ROS and disuse. Future studies should examine the specific mechanisms responsible for the rise in ROS production during disuse-induced skeletal muscle atrophy, as well as the notion of cross-talk among oxidant sources. In the ROS-induced ROS-release model described by Andreas Daiber (2010), activation of Nox and subsequent superoxide production could lead to depolarization of mitochondrial membrane ATP potassium channels. The reduction in mitochondrial membrane potential would then lead to increased mitochondrial-derived ROS, which could activate PKC. Active PKC has been shown to be capable of triggering Nox2 complex formation and activation. In this model, the initial ROS production from Nox2 signals for the augmentation and intensification of oxidative stress from the mitochondria (Daiber, 2010). In addition, activation of Fn14 has been shown to promote ROS production by stimulating Nox2 activity in macrophages (Madrigal-Matute *et al.*, 2015). Thus it is possible that Nox2 serves as an intermediate in an Fn14 – Nox2 – NFκB pathway. Clearly, there are many unanswered questions and continuing research efforts will be required to elucidate our understanding of both the locations and regulation of ROS production during disuse-induced skeletal muscle atrophy.

2.5 Potential Role of Neuronal Nitric Oxide Synthase-mu During Disuse Atrophy

Currently, we do not have a full understanding of the complexities involved in oxidant production during disuse-induced skeletal muscle atrophy. Skeletal muscle wasting that occurs during pathological conditions, such as sepsis and chronic heart failure, has been associated with an over-production of nitric oxide (•NO) (Adams *et al.*, 1997; Nin *et al.*, 2004). However, upregulation of the inducible nitric oxide synthase

(iNOS), rather than the neuronal nitric oxide synthase isoform (nNOS), was cited as causal in cachectic muscle atrophy.

However, during disuse-induced atrophy it is unclear whether excess •NO production, source, or localization accelerates the atrophic process. In a study by Suzuki et al. (2007), 14 days of hindlimb unloading was associated with a sarcoplasmic translocation of the mu (μ) – isoform of neuronal nitric oxide synthase (nNOSμ) from the sarcolemma-localized dystrophin glycoprotein complex (DGC), and this translocation correlated with elevated levels of sarcoplasmic •NO (Suzuki *et al.*, 2007). Their group followed this experiment up with genetic and pharmacological nNOS inhibition studies that indicated translocation of nNOSμ activity during hindlimb unloading as a critical event promoting atrophy (Suzuki *et al.*, 2007). Dystrophin remained attached to the DGC while dysferlin, a multifunctional protein involved in membrane repair, remained bound to nNOSμ. Inhibition of nNOS prevented activation of FoxO3a and ubiquitin ligases (Suzuki *et al.*, 2007). Cytosolic levels of •NO were elevated as determined via EPR (electron paramagnetic resonance). We found that nNOSμ translocation is an early event in the mechanical unloading process, occurring within 3 days with the rat model (Lawler *et al.*, 2014) In addition, Vitadello *et al.* (2014a) also found untethering of nNOSμ from the sarcolemma and translocation of nNOSμ with hindlimb unloading, linked to downregulation of grp94 (Vitadello *et al.*, 2014b). Grp94 is an HSP90-like stress protein that chaperones protein folding (Marzec *et al.*, 2012).

In contrast, Lomonosova *et al.* (2011) reported that L-arginine mitigated hindlimb unloading-induced reduction of nNOS, •NO, dystrophin, and HSP90 protein levels and mRNA transcripts gene expression. Heterogeneity in dystrophin sarcolemmal localization was found, suggesting disruption of the DGC. Furthermore, hindlimb unloading reduced levels of desmin (Lomonosova *et al.*, 2011), a z-disc fiber protein that transmits loading to the DGC and surrounding extracellular matrix protein (e.g., laminin, collagen). Protein abundance was determined from serial frozen cross-sections, and thus assessed global levels, rather than site-specific changes. Efficacy of L-arginine may suggest a substrate limitation or de-coupling of nNOSμ. In addition, a different spin trap was used for EPR in the Lomonosova study compared with Suzuki *et al.*: diethyl-dithiocarbamate (DETC) vs. *N*-methyl-D-glucamine-dithiocarbamate (MGD). Thus the global role of •NO and downstream nitrosative species remain uncertain in unloading induced atrophy. However, we propose that (1) disruption of the DGC and membrane environment and untethering of nNOSμ from the sarcolemma, (2) subcellular location of nNOS and downstream effects on FoxO3a-ubiquitin ligase signaling, (3) substrate availability, (4) the role of other NOS isoforms, and (5) local •NO bioavailability may be more important than global •NO levels in regulating muscle fiber atrophy with mechanical unloading. However, additional research is crucial to unraveling these mysteries.

Interestingly, evidence indicates NOS and •NO are involved in the regulation of the type I MHC isoform (Sellman *et al.*, 2006; Suwa *et al.*, 2015). For instance, a recent report found that with 8 weeks of NOS inhibition there was a significant decrease in the

percentage of type I fibers and concomitant increase in the percentage of type IIa fibers in the soleus muscle (Suwa *et al.*, 2015). Since disuse leads to a shift in fiber type from type I to type IIa, those data point towards the notion that a reduction in myofiber •NO may be a critical event promoting the shift.

It is proposed that in healthy muscle sarcolemma-localized nNOSμ is required for myofiber mechanotransduction. For example, muscle fiber hypertrophy with mechanical overloading was dependent upon intact sarcolemmal nNOSμ and NADPH oxidase 4 (Nox4) (Ito *et al.*, 2013). Genetic ablation or inhibition of nNOSμ early in the overloading process attenuated muscle hypertrophy by over 50% (Ito *et al.*, 2013). In support of these findings, the reduction in sarcolemma nNOSμ that occurs with unloading leaves the muscle fiber susceptible to sarcolemma lysis by neutorphils upon reloading (Nguyen & Tidball, 2003), thus slowing recovery. Whereas, mice expressing a muscle-specific nNOS transgene were significantly protected from sarcolemma damage and injury in response to reloading (Nguyen & Tidball, 2003). Clearly, nNOSμ plays a vital role as a load sensitive molecule in skeletal muscle. Translocation of nNOSμ has been reported to occur in response to various forms of disuse: hindlimb unloading (Tidball *et al.*, 1998; Suzuki *et al.*, 2007; Lawler *et al.*, 2014), spaceflight (Sandona *et al.*, 2012), denervation (Suzuki *et al.*, 2007), bed rest (Rudnick *et al.*, 2004), and intensive care-associated critical illness myopathy (Llano-Diez *et al.*, 2012). While some have observed disuse-induced alterations in nNOSμ synthesis and/or degradation, the mislocalization of nNOSμ in postural muscles is a common event associated with atrophy. Suzuki et al. (2007) observed a causal link between nNOSμ untethering and

proteolytic FoxO3a activation during hindlimb unloading. Our group demonstrated that administration of a superoxide dismutase (SOD) / catalase mimetic (EUK134) reduced the extent of nNOSμ untethering from the sarcolemma and translocation to the sarcoplasm following 54 hours of hindlimb unloading (Lawler *et al.*, 2014). This effect attenuated the activation of FoxO3a, subsequent atrophy and shift in fiber type in the soleus muscle (Lawler *et al.*, 2014). In support of these observations, mice treated with curcumin, which contains antioxidant and anti-inflammatory properties, mitigated nNOSμ translocation and atrophy (Vitadello *et al.*, 2014a). Those data suggest that disuse-induced translocation of nNOSμ is due in part to a rise in oxidative stress.

Much remains to be learned concerning the many roles of nNOSμ during mechanical unloading. For example, further examination is needed to elucidate whether translocated nNOSμ leads to elevated localized •NO within the sarcoplasm of the fibers and which signaling pathways are affected. Does nitrosylation of glutathione play a role in dephosphorylation of FoxO3a? What are the mechanisms of substrate limitation? What are the mechanisms underlying redox regulation of nNOSμ during unloading? A causal link between nNOSμ translocation is directly associated with depressed protein synthesis is also of interest. In addition, identifying the molecular mechanisms guiding nNOSμ untethering from dystrophin and alpha-syntrophin in the DGC are of significant concern. In addition, are the effects of nNOSμ translocation fiber type-dependent? Does nNOSμ translocation trigger fiber-type switch from slow to fast-twitch with unloading?

2.6 Conclusions

In summary, disuse-induced skeletal muscle atrophy is due in part to the stressful myofiber environment caused by elevations in ROS. Oxidative stress is implicated as a mechanism for blunted rates of muscle protein synthesis and increased proteolysis (*summarized in* **Figure 2.2**). Various myofiber oxidant sources participate in the production of ROS and are potentially involved in a ROS-induced ROS-release feedback mechanism. In addition, future studies are needed to determine the specific upstream signaling events that trigger the disuse-induced ROS production from each oxidant source. While the data remains unclear concerning •NO production during disuse, there is a better understanding of the link between atrophying muscle and nNOSμ translocation. However, future studies are needed to elucidate the connections between oxidative stress, nNOSμ translocation, and the affected atrophic signaling cascades.

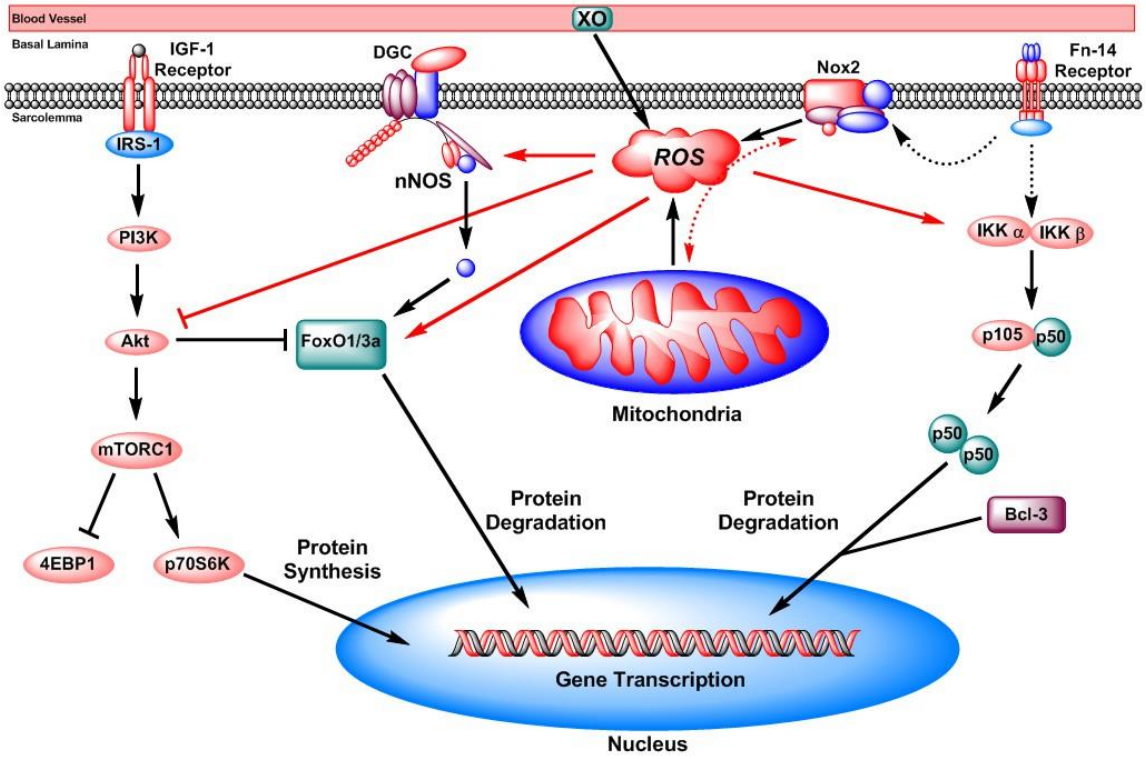

Figure 2.2. Critical signaling pathways controlling muscle fiber size during disuse-induced atrophy and the regulatory schemes exerted by ROS. The combination of reactive oxygen species (ROS) derived from mitochondria, NADPH oxidase isoform 2 (Nox2), and xanthine oxidase (XO) results in an increased ROS concentration in myofibers during periods of disuse. Elevated ROS can blunt Akt-mTORC1 protein synthesis signaling, induce dislocation of nNOSμ from the DGC towards the sarcoplasm, enhance dephosphorylation of FoxO1/3a, and promote NFkB signaling. In addition, ROS from Nox2 and/or mitochondria may promote a ROS-induced ROS-release amplification scheme (as shown by the dashed red-line with arrowheads). ROS regulatory functions are shown with red lines. Dashed lines indicate hypotheses concerning signaling events made by the authors based on published research findings. This is a simplified figure illustrating ROS-regulation of disuse fiber atrophy; refer to text for brief discussions on alternative pro-degradation routes (e.g. calpains, caspase-3, autophagy-lysosomal).

CHAPTER III

AT1 RECEPTOR BLOCKADE ATTENUATES HINDLIMB UNLOADING-INDUCED MODIFICATIONS OF NOX2, NNOS, AND FOXO3A SIGNALING IN SKELETAL MUSCLE

3.1 Introduction

Maintenance of skeletal muscle mass and function is critical for our overall health and quality of life. The result of prolonged periods of disuse, such as forced bedrest, limb casting, and spaceflight, is a loss of skeletal muscle mass. While there are various forms of disuse, the underlying cellular mechanisms share some similarities. Skeletal muscle atrophy is primarily due to an imbalance in muscle protein turnover, characterized by a reduction in protein synthesis and an upregulation in protein degradation (Schiaffino *et al.*, 2013). Understanding the various pathways involved in the blunted synthesis and elevated degradation rates leading to disuse-induced skeletal muscle atrophy is imperative to making progress towards therapeutic interventions that aim to mitigate, delay, or even prevent atrophy.

The protein synthesis vs. degradation imbalance is due in part to blunting of Akt / mTORC1 signaling and increased activity of the various proteolytic pathways (Schiaffino *et al.*, 2013; Egerman & Glass, 2014). The primary degradation pathways involved in disuse atrophy are the ubiquitin proteasome pathway (UPP), the calcium-dependent caspase-3 and calpains, and the autophagy-lysosomal pathway (Powers *et al.*, 2007; Schiaffino *et al.*, 2013). A critical signaling event during disuse atrophy is the

activation of forkhead members of the class O (FoxO) transcription factors (i.e., FoxO1/3a). FoxO1/3a are implicated in the regulation of myofiber size through transcriptional regulation of atrogenes such as ubiquitin E3 ligases, muscle-specific RING finger protein 1 (MuRF1) and muscle atrophy F-box (MAFbx) / atrogin-1 (Bodine *et al.*, 2001; Schiaffino *et al.*, 2013). Along with FoxO1/3a, recent evidence indicates that ATF4 and p53 function as transcription factors during short-term disuse, promoting the expression of growth-arresting proteins ((Fox *et al.*, 2014). The extent to which the various pathways are involved in disuse atrophy depends the type of disuse, length of disuse, and fiber composition of the muscle.

Prolonged periods of disuse are associated with increased production of reactive oxygen species (ROS) in skeletal muscle fibers (Kondo *et al.*, 1993; Lawler *et al.*, 2003). The disuse-induced elevation in oxidative stress is theorized to be a trigger of atrophic signaling. Three oxidant sources linked to disuse atrophy include ROS from the electron transport chain in mitochondria (Min *et al.*, 2011; Talbert *et al.*, 2013b), xanthine oxidase (XO) (Matuszczak *et al.*, 2004; Derbre *et al.*, 2012), and NADPH oxidase (Nox) (Lawler *et al.*, 2014). While mitochondria are likely the primary source of ROS during disuse (Min *et al.*, 2011), the contribution of XO and Nox cannot be overlooked. Skeletal muscle cells are known to have two Nox isoforms: Nox2 (Semprun-Prieto *et al.*, 2011; Lawler *et al.*, 2014) and Nox4 (Sun *et al.*, 2011). Nox2 is a multi-subunit complex that consists of two membrane-bound subunits (gp91phox and p22phox) and four cytosolic subunits (p40phox, p47phox, p67phox, and Rac-1). Nox2 complexes become active when the cytosolic subunits join the sarcolemmal subunits and convert oxygen to

the superoxide radical, as depicted in **Figure 3.1**. We recently reported that 54 hours of hindlimb unloading was associated with increased sarcolemmal content of two Nox2 subunits, gp91phox and p47phox (Lawler *et al.*, 2014). In addition, Nox inhibition attenuates disuse-induced contractile dysfunction and fiber atrophy in the rodent mechanical ventilation model (McClung *et al.*, 2009). Activation of Nox2 appears to be dependent upon Rac-1 activation and protein kinase C (PKC) activation of p47phox (Balakumar & Jagadeesh, 2014). Upstream signaling events include angiotensin II (AngII) ligand-binding of the AngII type 1 receptor (AT1R) which leads to phosphorylation of PKC and subsequent Nox2 activity (Balakumar & Jagadeesh, 2014). Furthermore, exposure of skeletal muscle cells to elevated levels of AngII is known to result in atrophy (Semprun-Prieto *et al.*, 2011; Kadoguchi *et al.*, 2015). Moreover, in the rat model of hindlimb unloading, plasma AngII is significantly increased following 7 days of disuse (Chung *et al.*, 2012).

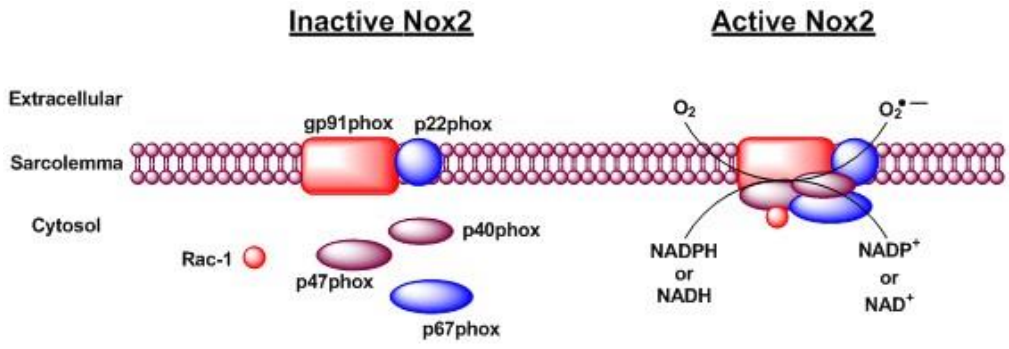

Figure 3.1. Illustration of inactive versus active Nox2 complex formation. Active conformation requires cytosolic components to join the membrane bound subunits.

Our previous findings have also established a link between the disuse-induced increase in ROS production and the translocation of sarcolemma-localized neuronal nitric oxide synthase (nNOS) to the sarcoplasm (Lawler *et al.*, 2014). Translocation of nNOS occurs in a variety of disuse models, and the rise in sarcoplasmic nNOS content has been implicated in the dephosphorylation / activation of FoxO3a (Suzuki *et al.*, 2007; Llano-Diez *et al.*, 2012; Sandona *et al.*, 2012; Lawler *et al.*, 2014), as illustrated in **Figure 3.2**. We have postulated that elevated Nox2-derived ROS occuring during disuse is critical to the nNOS dislocation and subsequent activation of FoxO3a and, therefore, the resulting atrophy.

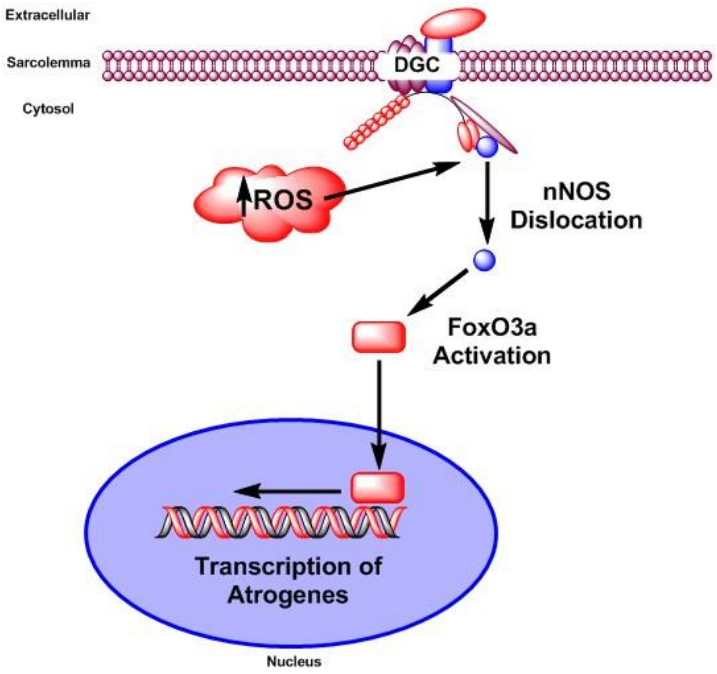

Figure 3.2. Illustration of the consequence of mechanical unloading-induced rise in ROS and subsequent nNOS untethering from the sarcolemma localized dystrophin glycoprotein complex (DGC).

In the present study, we evaluated the effects of AT1R blockade in hindlimb unloaded rats on soleus muscle morphology, fiber type, oxidative stress, and markers of skeletal muscle atrophy. We hypothesized that administration of the AT1R antagonist, losartan, would mitigate the negative effects associated with mechanical unloading, such as reduction in muscle fiber cross-sectional area, slow-to-fast fiber type shift, elevated ROS production, accumulation and activation of Nox2, nNOS translocation, and nuclear localization of pro-atrophy transcription factors (*summarized in* **Figure 3.3**).

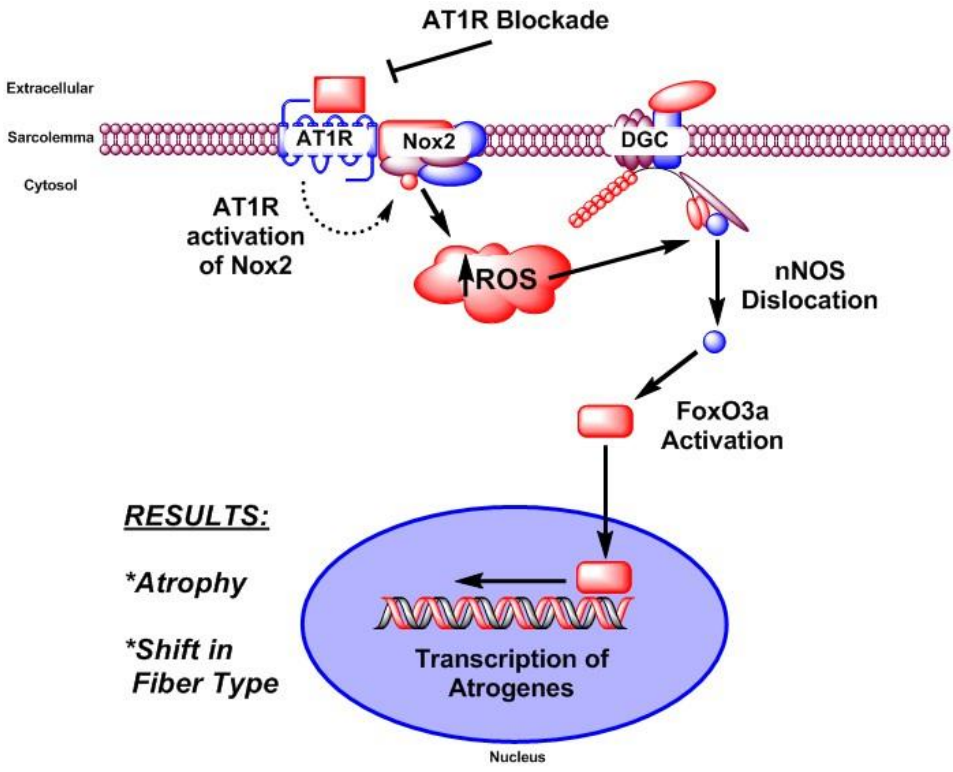

Figure 3.3. Proposed model of the influence of AT1R activation during hindlimb unloading-induced atrophy.

3.2 Materials and Methods

3.2.1 Animals

All animal procedures were approved by the Institutional Animal Care and Use Committee (IACUC) at Texas A&M University. Young adult (4-5 months) Fischer-344 (F344) rats were subjected to skeletal muscle disuse via hindlimb unloading. Animals were housed and cared for in accordance with the National Institutes of Health policy (NIH: DHEW publication no. 85-23, revised 1985). Rat chow (4% fat) and water were provided *ad libitum*, and the animals were maintained in a temperature-controlled room (23 ± 2°C) with a 12:12 hour light-dark cycle. Rats are valuable models for the examination of skeletal muscle wasting that occurs during disuse and unloading in humans, with disuse-induced responses such as changes in muscle fiber cross-sectional area, weakness and fiber type shifting from slow to fast common to both the rat and human responses.

3.2.2 Hindlimb Unloading

Systemic physiological effects of microgravity and bed rest are accurately replicated in the ground-based hindlimb unloading model. An adaptation of the rodent tail-suspension hindlimb unloading model (Globus & Morey-Holton, 2016) was utilized to induce mechanical unloading. Rats were anesthetized with an intraperitoneal (i.p.) injection of a ketamine (75 mg/kg) / xylazine (10 mg/kg) cocktail solution to induce unconsciousness, dampened sensations, and muscle relaxation allowing research personnel to harness the tail. Tail harnesses were then connected to a cross-wire that spanned across the top of the cage. The hindlimbs of the rats were lifted so that their

hindfeet were approximately 1 mm off of the cage floor. Hindlimbs of the rats remained unloaded for a total of 7 days. At the end of the 7-day period, rats were sacrificed. Rats were euthanized with 120 mg/kg i.p. sodium pentobarbital (Euthanasia III Solution).

3.2.3 Experimental Design

A hindlimb unloading duration was chosen to target the early stages of skeletal muscle remodeling during disuse. Markers of atrophy and oxidative stress have been observed to peak or be near a peak state at the 7-day time point during disuse (Dupont *et al.*, 2011). We used a United States Food and Drug Administration (FDA)-approved angiotensin II type 1 receptor blocker, losartan, as an intervention to target the potential upstream trigger of oxidative stress during disuse. Adult F344 rats were divided into four groups (n = 7 / group): loaded controls (CON), 7 days of hindlimb unloading (HU), 7 days of HU + 40 mg/kg/day i.p. of losartan (HUL), and loaded controls + losartan (CONL). Please refer to the **Appendix** for justification of the losartan dosage used in this study. CON and HU rats received daily i.p. injections of similar volumes of physiological saline. Administration of losartan or saline began 24 hours prior to hindlimb unloading and continued throughout the 7-day unloading period (8 days total). Sample size calculations were based on soleus muscle fiber cross-sectional area, which has the lowest mean percentage difference among our results in preliminary studies.

3.2.4 Skeletal Muscle Tissue Preparation

The soleus muscle was chosen as a model of skeletal muscle response to mechanical unloading disuse. As a postural muscle with a high percentage of Type I (slow twitch) fibers, the soleus is susceptible to rapid atrophy and remodeling when

exposed to mechanical unloading (Ohira *et al.,* 1992). Rats were euthanized with 120 mg/kg of pentobarbital sodium salt (Euthanasia III Solution) by way of an i.p. injection. The soleus muscles were extracted, trimmed of excess tissue, rinsed with phosphate-buffered saline (PBS) solution and laid longitudinally on a polyurethane mount of tissue freezing medium before being frozen in liquid nitrogen-cooled isopentane (2-Methylbutane). Samples were subsequently stored at -80°C until needed for the following experimental techniques or assays.

3.2.5 Subcellular Fractionation

Soleus muscles were minced, weighed, and washed with cold PBS prior to homogenization. Subcellular fractionation was performed using adaptations of the methods described by (Brenman *et al.*, 1995) and (Dimauro *et al.*, 2012) (*summarized in* **Figure 3.4A**). Soleus samples were homogenized in lysis *Buffer A* (10:1 w/v) containing the following: 25 mM Tris-HCL, pH 7.4, 100 mM NaCl, 1 mM EDTA, 1 mM EGTA, and protease inhibitor cocktail. Muscles were homogenized using a motorized ground glass-on-ground glass mortar and pestle at 4°C. Nuclei and debris were pelleted by centrifugation at 1,000x*g* for 10 minutes. The resulting supernatant was then centrifuged at 20,000x*g*. The resulting supernatant was the cytoplasmic fraction while the remaining pellet was re-suspended in *Buffer A* and deemed the crude-microsomal/membrane fraction.

The nuclear fraction was isolated as described by Dimauro et al. (2012) with minor modifications. Nuclei and debris pelleted following centrifugation at 1,000x*g* (as noted in the previous paragraph) was re-suspended in *Buffer B* (6:1 w/v) which

contained 250 mM sucrose, 50 mM Tris-HCL pH 7.4, 5 mM $MgCl_2$, and protease inhibitor cocktail, vortexed and then centrifuged at 500x*g* for 15 minutes. The resulting supernatant was discarded and the pellet was re-suspended in *Buffer B*, vortexed and then centrifuged at 1,000x*g* for 15 minutes. Once again, the supernatant was discarded and the pellet was re-suspended in *Buffer C* (20 mM HEPES pH 7.9, 1.5 mM MgCl2, 0.5 M NaCl, 0.2 mM EDTA, 20% glycerol, 1% Triton-X-100, protease inhibitor cocktail). This fraction incubated on ice for 30 minutes and was intermittently vortexed. Next, the fraction was centrifuged at 9,000x*g* for 30 minutes, and the resulting supernatant was deemed the nuclear fraction.

Protein concentrations were determined using the Bradford protein assay, following the manufacturer's instructions (Bio-Rad, cat # 500-0006). Tissue extracts were subsequently aliquoted and stored at -80°C until western blot analysis. Validation of each subcellular fraction was assessed by western blotting (**Figure 3.4B**) for GAPDH (cytoplasmic) (1:10,000, EMD Millipore, cat # MAB374), Na^+/K^+ ATPase α-1 (crude membrane) (1:1,000, EMD Millipore, cat # 05-369), and Histone H3 (nuclear) (1:1,000, Cell Signaling Technology, 9715).

3.2.6 Western Blotting

Soleus muscle extracts (20 µg or 30 µg) along with sample buffer were loaded into wells of 8% or 10% SDS-PAGE gels. Electrophoresis was conducted at 120 V for ~75 min. Gels were then transferred at 100 V for ~60 min onto a nitrocellulose

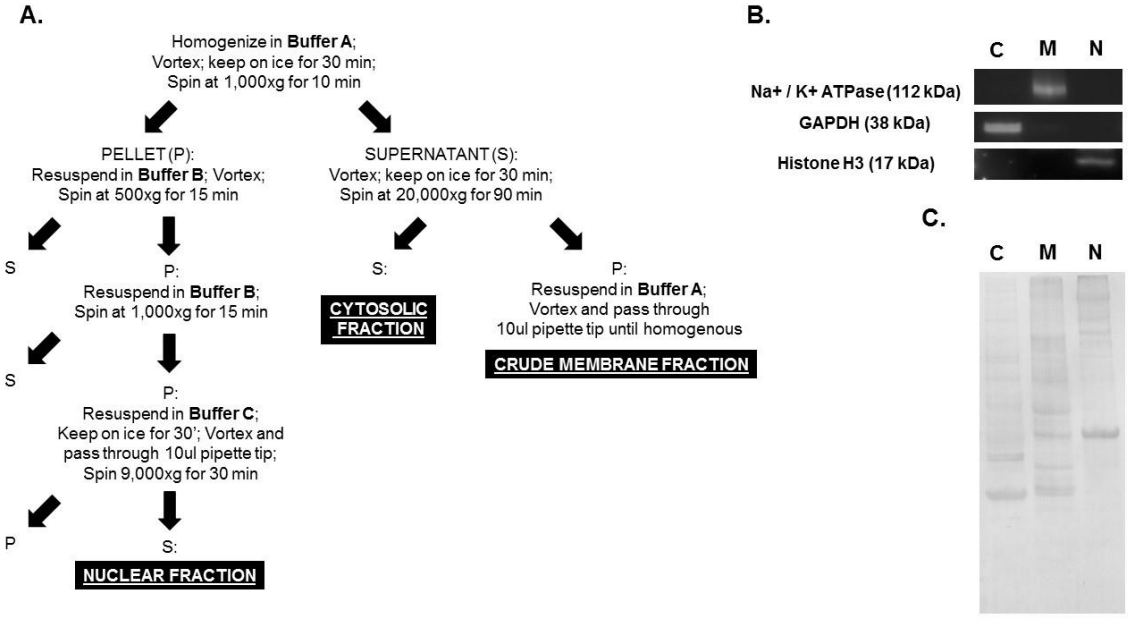

Figure 3.4. Validation of subcellular fractionation preparation. Soleus muscle lysates were used to isolate the membrane, cytosolic, and nuclear subcellular fractions. ***A,*** flow chart of the fractionation protocol. ***B,*** detection of the various proteins. Western blot detection of Na+/K+ ATPase, GAPDH, and Histone H3 were used to confirm the membrane, cytosolic, and nuclear fractions, respectively. ***C,*** the PVDF membrane stained with Ponceau S Red stain following the blotting procedures. Each lane contained 30µg of protein: cyotosolic (C) fraction in lane 1, Membrane (M) fraction in lane 2, and nuclear (N) fraction in lane 3.

membrane (Bio-Rad, cat # 162-0112). Membranes were blocked in a non-fat milk buffer (5% non-fat milk in TBS) for 1 h. Following blocking, membranes incubated overnight (4°C) in blocking buffer with the appropriate primary antibody: anti-nNOS (1:750, Life Technologies, cat # 61-700), anti-gp91phox (1:1000, BD Biosciences, cat # 611415), anti-p67phox (1:2500, BD Biosciences, cat # 610913), anti-p47phox (1:750, BD Biosciences, cat # 610355), anti-Rac1 (1:500, EMD Millipore, cat # 07-1464), anti-FoxO3a (1:750, Cell Signaling Technology, cat # 12829), and anti-p53 (1:750, Cell

Signaling Technology, cat # 2527). Membranes were subsequently washed in tris buffered saline (TBS) with 0.1% Tween-20 (TBS-T) (3 x 5 min) and then incubated at room temperature for 1 h in blocking buffer containing the appropriate HRP-conjugated secondary antibodies (Santa Cruz Biotechnology, cat # sc-2004 or sc-2005). After TBS-T washes, proteins were visualized by Super Signal West Dura Extended Duration Substrate (Thermo Scientific, cat # 34076) enhanced chemiluminescence detection and developed with the Fuji LAS-3000 Luminescent Image Analyzer (FujiFilm Medical Systems). Quantification was performed using NIH ImageJ software. Ponceau-S staining (cytoplasmic: band ~38 kDa mark (GAPDH); crude membrane: band ~42 kDa mark (actin); nuclear: band ~42 kDa mark (actin)) was used as a loading control.

3.2.7 Histological Analysis

Soleus muscles were embedded in tissue freezing medium and subsequently frozen. Muscles were cut in 10 µm sections from the midbelly of the muscle using a cryostat (Thermo Scientific, Shandon Cryotome FSE) and allowed to air-dry for 30 minutes. Hematoxylin and eosin (H&E) stains were used to assess tissue morphology and performed as previously described (Lawler *et al.*, 2014).

Muscle sections were also stained with wheat germ agglutinin (WGA) Alexa Fluor 555 conjugate (WGA-Alexa 555, 1:40, Life Technologies, cat # W32464) in order to visualize the sarcolemma and connective tissue. Sections were co-stained with a DAPI solution (1:500, Life Technologies, cat # D1306) for 5 min according to the manufacturer's guidelines. Slides were air-dried prior to coverslip mounting with Prolong Gold anti-fade medium (Life Technologies, Grand Island, NY).

NADPH-diaphorase histochemical analysis was used to examine the presence and localization of active nNOS. This assay was performed as previously described (Vitadello *et al.*, 2014b) with minor modifications. Ten µm soleus muscle sections were fixed for 20 min with 2% paraformaldehyde followed by a PBS wash. Sections were then incubated in a buffer containing 50 mM Tris-HCl pH 8.00, 0.2% Triton-X-100, 0.5 mM nitrotetrazolium blue chloride, and 1 mM β-NADPH for 2 h at 37°C. The enzymatic reaction was stopped by briefly rinsing the slides with distilled water and then allowed to air-dry. Coverslips were mounted onto the samples with permanent mounting medium (Vectamount, Vector Laboratories, cat # H-5000).

Stained sections were visualized and photographed with a Zeiss Axioplot upright microscope and Zeiss Axiocam HRc color camera (Carl Zeiss Microimaging, Thornwood, NY). Images from WGA stained cross-sections (n = 5 - 6 / group) were quantified using NIH ImageJ to determine the percentage of area positively stained by WGA, as well as the integrated density of the WGA stained portions. NADPH-diaphorase stained samples (n = 5 - 6 / group) were quantified by using NIH ImageJ to obtain the cross-sectional circumference (CSC) and determining the percentage of the sarcolemma that stained positively for NADPH-diaphorase.

3.2.8 Immunofluorescence

To examine protein localization, soleus muscle cross-sections obtained from the midbelly were serially sectioned at 10 µm thick in a cryostat at -15°C and placed onto microscope slides. Samples were fixed in either acetone (myosin heavy chain immunofluorescence) at -20°C for 10 min or in 2% paraformaldehyde followed by a 20

min incubation in citrate buffer at 92°C (nNOS and FoxO3a immunofluorescence). Following fixation, sections were washed in PBS with 0.1% Tween20 (PBS-T). Sections were blocked in a 10% normal goat serum (ThermoFisher Scientific, cat # 50062Z) for 15 min. After blocking, sections incubated in blocking buffer containing specific primary antibodies: dystrophin (1:100, Santa Cruz Biotechnology cat # sc-15376), slow skeletal myosin heavy chain (1:250, Abcam, cat # ab11083), fast skeletal myosin heavy chain (1:250, Abcam, cat # ab51263), nNOS (1:100, Cayman Chemical, cat # 160870), FOXO3a (1:50, Sigma-Aldrich, cat # SAB3500508), and Beta-Sarcoglycan (1:200, Abcam, cat # ab55683) for 1 hour in an enclosed chamber at room temperature. After three 5 min washes in PBS, sections were incubated in the appropriate secondary antibody with a fluorophore attached (e.g., goat anti-rabbit Alexa Fluor 488, goat anti-mouse Alexa Fluor 594) (1:200) for 30 min at room temperature. Sections were subsequently washed twice in PBS-T and once in PBS. Some instances required DAPI staining, which involved 5 min incubation followed by PBS washes. Slides were allowed to air-dry prior to mounting with Prolong Gold anti-fade medium (Life Technologies, Grand Island, NY). Images were captured on a Zeiss Axioplot upright microscope and Zeiss Axiocam HRc color camera.

Muscle fiber CSA was determined on β-sarcoglycan- and dystrophin-stained muscle cross sections by employing the semi-automatic muscle analysis using segmentation of histology (SMASH) MATLAB-based program (Smith & Barton, 2014). A range of 200-250 fibers per muscle were quantified to obtain an average CSA from each sample (n = 7 / group). Quantification of the percentage of FoxO3a positive

myonuclei was accomplished by triple staining soleus sections with anti-FoxO3a, anti-β-Sarcoglycan, and DAPI to determine the co-localization of FoxO3a with myonuclei. A minimum of 300 myonuclei were counted per muscle sample (n = 4 / group) to obtain the percentage of FoxO3a positive myonuclei.

3.2.9 Oxidative Stress Marker

ROS generation was determined via a dihydroethidium (DHE) fluorescence protocol on soleus cross-sections. DHE is oxidized by superoxide to produce a fluorescent ethidium. Soleus muscle sections (10 µm) were air-dried and re-hydrated with PBS. Sections then incubated with 5 µmol DHE (Life Technologies, cat # D1168) in a dark, humidified chamber for 30 min at 37°C. Muscle sections were washed with PBS, air-dried and mounted with ProLong Gold Anti-fade mounting medium. Immediately after mounting the coverslips, images taken at 10x magnification were obtained using the Zeiss Axioplot microscope and HRc color camera. Ethidium-positive nuclei were quantified using particle analysis functions on NIH ImageJ. Four images taken at 10x magnification were quantified per sample (n = 6).

NADPH-dependent superoxide production was assessed with the lucigenin chemiluminescent assay (Heymes *et al.,* 2003; Whitehead *et al.,* 2010). Soleus muscle tissues were pooled together (n = 3 per pool) and homogenized in ice-cold buffer containing 25 mM Tris-HCL, pH 7.4, 100 mM NaCl, 1 mM EDTA, 1 mM EGTA, and a protease inhibitor cocktail. Protein concentrations of the total homogenate were determined by Bradford assay. Experiments were performed on a microplate luminometer (BioTek Synergy 4 Microplate Reader; 37°C) using 100 µg protein per

well, NADPH (300 µM) and lucigenin (10 µM). In order to confirm that the signal was due to superoxide production, a superoxide dismutase mimetic (EUK-134, 50µM, Cayman Chemical, cat # 10006329) was used to scavenge superoxide. In addition, pharmacological inhibitors were used to confirm that the activity was primarily due to NADPH oxidase: the non-specific NADPH oxidase inhibitor diphenyleneiodonium (DPI, 10 µM, Sigma-Aldrich, cat # D2926) and the selective (Csanyi *et al.*, 2011) Nox2 inhibitor gp91ds-tat (5 µM, BioSynthesis, Inc., Lewisville, TX).

3.2.10 Statistical Design

All data reported here are as mean ± SEM. Statistical analysis was performed using GraphPad 6 software (GraphPad Software, Inc. San Diego, CA). One-way ANOVA was used to identify differences among CON, HU, HUL, and CONL. Tukey's post-hoc analysis was utilized when necessary. Significance level for all tests was set at $p < 0.05$.

3.3 Results

3.3.1 Hindlimb Unloading-Induced Alterations in Soleus Muscle Morphology, but not Soleus Mass, are Mitigated by AT1R Blockade.

We tested the hypothesis that AT1R blockade would ameliorate the hindlimb unloading-induced morphological alterations in soleus muscles. A previous study found that AT1R blockade offers protection against limb-stapling-induced atrophy in sarcopenic mice (Burks *et al.*, 2011); however, we currently do not know if AT1R blockade is effective at preventing unloading-induced fiber atrophy in young, adult rats. In the current study, we found that seven days of hindlimb unloading resulted in a

significant drop in body weight compared to the control group (287.1 g vs 342.1 g; p = 0.003) (**Table 3.1**). Administration of losartan during HU did not offer significant protection against the HU-induced reduction in body weight (299 g vs 287.1 g; p = 0.826). In addition, soleus muscles from HU rats were significantly smaller than those from controls (103 mg vs 123.1 mg; p = 0.001) (**Table 3.1**). Soleus muscles from HUL rats were not significantly protected from the HU-induced drop in muscle weight (106.8 mg vs 103 mg; p = 0.8687). Ambulatory control rats that received losartan (CONL) did not differ from CON rats in body weight (p = 0.999) or soleus weight (p = 0.9043).

Groups	Body Weight (g)	Soleus Weight (mg)	Soleus Weight / Body Weight (mg / g)
CON	342.1 ± 10.30	123.1 ± 2.133	0.3605 ± 0.004
HU	287.1 ± 8.983 [ad]	103.0 ± 3.812 [ad]	0.3587 ± 0.015
HUL	299.0 ± 6.453 [ad]	106.8 ± 4.259 [ad]	0.3557 ± 0.011
CONL	343.0 ± 12.49	126.5 ± 3.491	0.3603 ± 0.006

Table 3.1. Effect of AT1R blockade on body weight, soleus muscle weight, and soleus muscle weight / body weight in control and hindlimb unloaded rats. Body weight is expressed in grams (g). Soleus weight is expressed in milligrams (mg). Data are expressed as mean ± SEM. Values sharing the same letter are not significantly different ($p < 0.05$): [a] indicates different from CON; [d] indicates different from CONL.

Quantification of the average cross-sectional area (CSA) of the soleus muscles indicates that unloading resulted in a significant reduction of 34% in myofiber CSA compared to ambulatory controls (3469 μm^2 vs 2291 μm^2; $p < 0.0001$). Losartan

administration offered significant protection against unloading-associated reduction in fiber CSA (2996 μm^2 vs 2291 μm^2; $p = 0.001$), but still remained significantly smaller than CON ($p = 0.0328$). The majority of fibers in HU muscles were in the 1000 - 3000 μm^2 range (84.5%), whereas 83.8% of the CON fibers were found in the 2000 – 4500 μm^2 range. Fibers from the HUL muscles were predominately in the 1000 – 4500 μm^2 range (85.9%), exhibiting a wider range of fiber CSA than the HU muscles (**Figure 3.5A**). Interestingly, we found that losartan reduced unloading-induced muscle fiber atrophy primarily in Type I fibers (3436 μm^2 v. 2257 μm^2; $p = 0.0002$) but did not offer protection in Type II fibers (2203 μm^2 v. 1931 μm^2; $p = 0.4668$) (**Figure 3.5B**). Fiber CSA from CONL rats did not differ from CON rats in fiber CSA.

Additionally, we assessed whether the mechanical unloading-induced shift of soleus muscle fiber type from slow to fast (i.e., Type I to Type II) was impacted by AT1R blockade. Representative immunofluorescent fiber-type specific stains are shown in **Figure 3.6A**. As expected, unloading resulted in a significant reduction in the percentage of Type I fibers compared to CON (75.41% vs 88.34%; $p < 0.0001$) (**Figure 3.6B**), concomitant with a significant increase in the percentage of Type II fibers (24.59% vs 11.66%; $p < 0.0001$) (**Figure 3.6C**). These effects were mitigated with losartan administration; however, HUL soleus muscle fiber type composition still remained significantly different from CON, with a 6.46% difference ($p = 0.0015$) (**Figure 3.6B & C**). Soleus muscle fiber type composition did not differ between CON and CONL rats.

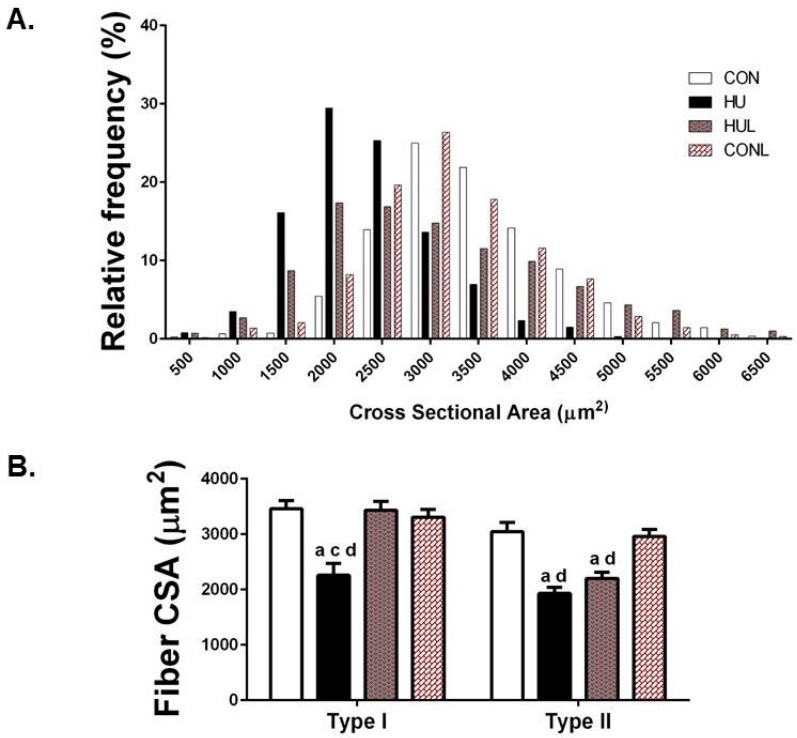

Figure 3.5. AT1R blockade mitigates soleus muscle fiber atrophy for Type I but not Type II fibers due to one week of hindlimb unloading. ***A,*** Distribution of muscle fibers according to fiber cross-sectional area (CSA) for controls (CON), hindlimb unloaded (HU), hindlimb unloaded + losartan (HUL), and control + losartan (CONL) *(n* = 7 / group). ***B,*** Average CSA for each group. ***C,*** Muscle fiber CSA by fiber type. Values are means ± SEM. Values sharing the same letter are not significantly different ($p < 0.05$): [a] indicates different from CON; [c] indicates different from HUL; [d] indicates different from CONL.

Through the use of wheat germ agglutinin (WGA) to visualize connective tissue in soleus muscle cross-sections, we found a significant 42.2% increase in extra-myofiber tissue area due to hindlimb unloading ($p < 0.0001$) (**Figure 3.7A & B**). Furthermore, HU led to a significant increase of 23% in WGA fluorescent intensity ($p < 0.0001$) (**Figure 3.7C**), indicative of an elevated concentration of connective tissue. Losartan treatment resulted in an anti-fibrotic effect, preventing the hindlimb unloading-induced

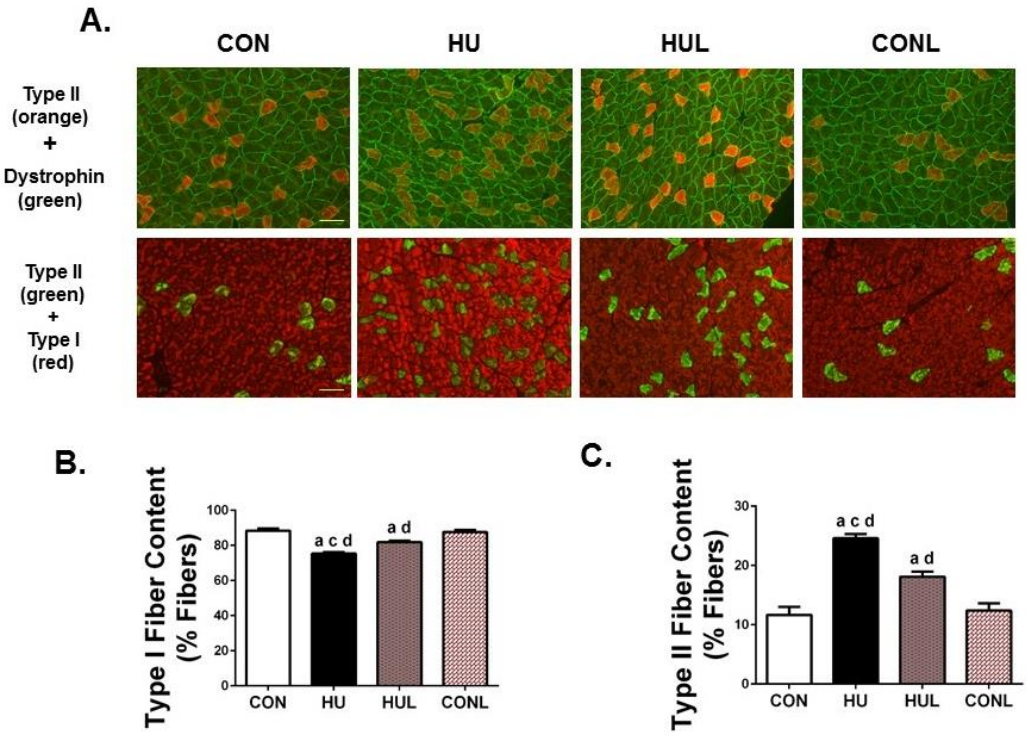

Figure 3.6. Hindlimb unloading-induced shift in fiber type is reduced in losartan treated rats. ***A (top row),*** representative immunofluorescence images of soleus muscles stained for type II muscle fibers (orange) and dystrophin (green); ***(bottom row),*** images of soleus muscles stained for type II muscle fibers (red) and type I muscle fibers (green). Scale bar = 100 μm. ***B,*** percentage of soleus muscle fibers that are type I fibers. ***C,*** percentage of muscle fibers that are type II fibers. Values are means ± SEM. Values sharing the same letter are not significantly different ($p < 0.05$): [a] indicates different from CON; [c] indicates different from HUL; [d] indicates different from CONL.

accumulation of connective tissue in both area ($p < 0.0001$) (**Figure 3.7B**) and intensity ($p = 0.0024$) (**Figure 3.7C**). Once again, build-up of extra-myocyte components were not significantly different between CON and CONL groups.

3.3.2 Increased ROS Production During Hindlimb Unloading is Partially Prevented by Losartan Treatment

In the next set of experiments, we tested the hypothesis that hindlimb unloading-

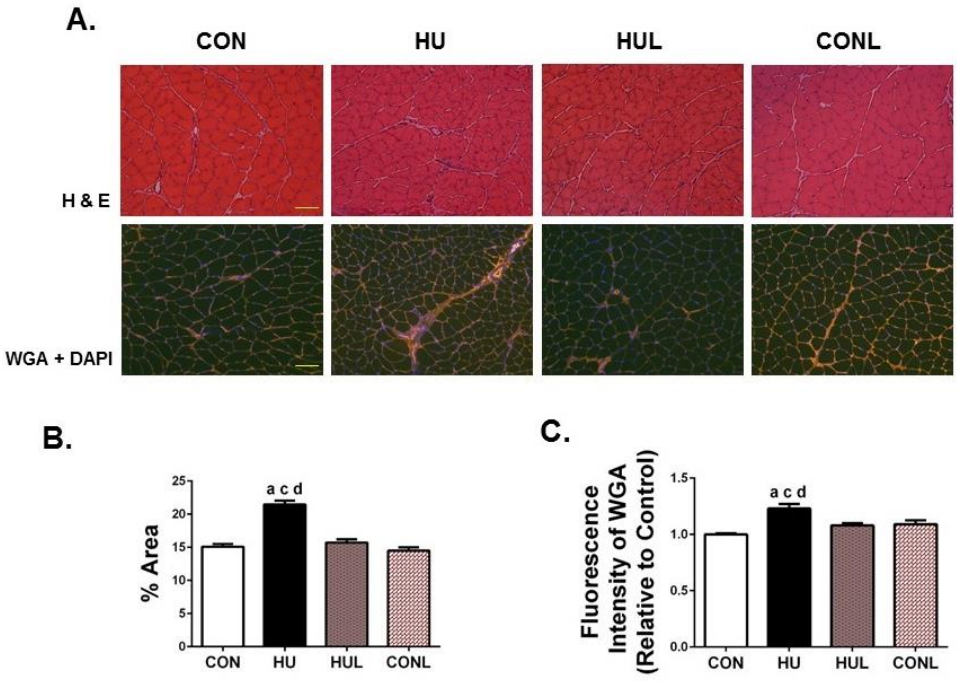

Figure 3.7. Mechanical unloading leads to an increase in connective tissue. ***A (top row),*** representative images of hematoxylin & eosin (H&E) stained soleus muscles; ***(bottom row),*** representative images of muscles stained for wheat germ agglutinin (WGA) and DAPI. Scale bar = 100 µm. ***B,*** quantification of the percentage of area positively stained by WGA per image. ***C,*** quantification of the fluorescence intensity of WGA. Values are presented as fold control of mean ± SEM. Values sharing the same letter are not significantly different ($p < 0.05$): [a] indicates different from CON; [c] indicates different from HUL; [d] indicates different from CONL.

induced production of reactive oxygen species would be reduced, primarily via Nox2 inhibition, by daily losartan administration. Soleus muscle cross-sections were incubated with dihydroethidium (DHE) to assess superoxide production. We found a significant rise in the number of nuclei positively stained with ethidium in HU cross-sections compared to the CON muscles ($p < 0.0001$) (**Figure 3.8**). In addition, we observed a significant protection offered by losartan treatment during unloading ($p = 0.0416$).

However, HUL still contained a significantly greater amount of ethidium positive nuclei compared to CON and CONL ($p = 0.0001$ and $p = 0.0091$, respectively).

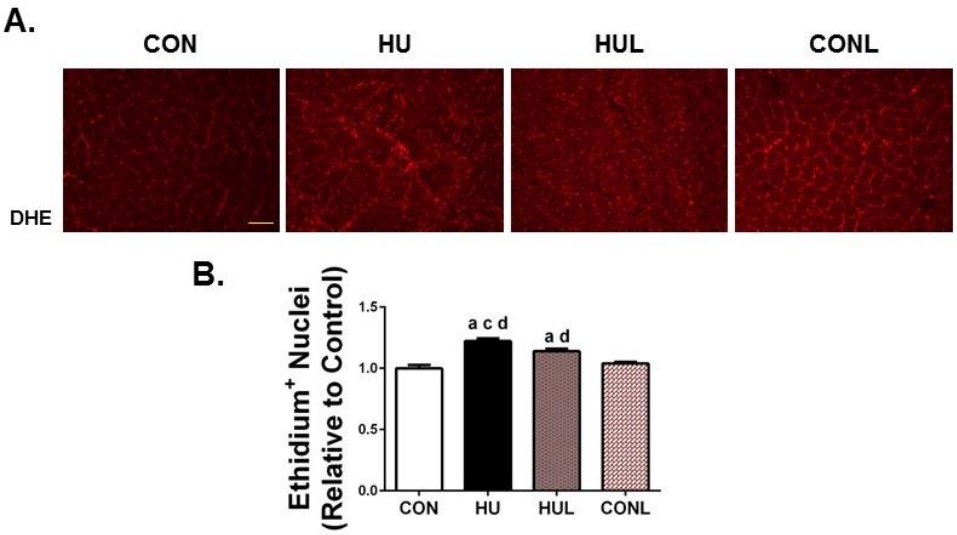

Figure 3.8. Hindlimb unloading leads to a rise in superoxide production. ***A,*** representative images of soleus muscle sections that were incubated with dihydroethidium (DHE) to indicate superoxide production. Scale bar = 100 µm. ***B,*** quantification of nuclei positively stained with ethidium. Values are presented as fold control of mean ± SEM. Values sharing the same letter are not significantly different ($p < 0.05$): [a] indicates different from CON; [c] indicates different from HUL; [d] indicates different from CONL.

Given that the hindlimb unloading-induced elevation in superoxide production was mitigated by losartan treatment and previous findings have observed that AT1R blockade ameliorates NADPH oxidase accumulation and production of superoxide, we measured the protein content of Nox2 subunits in the membrane fraction of the soleus muscle fibers. Western blot experiments showed a significantly greater content of the

membrane-bound gp91phox Nox2 subunit in HU samples compared to CON ($p = 0.0105$) (**Figure 3.9**). This effect was prevented by losartan treatment during HU with only a 28% rise in gp91phox content compared to CON, while remaining 60% lower than HU ($p = 0.1192$). Examination of sarcolemma-localized content of the transportable, cytosolic subunits found consistently increased trends among p67phox and p47phox subunits in HU compared to CON (79% and 88.7% increases, respectively) (**Figure 3.9**). In addition, a significant increase in sarcolemma content of Rac1 was observed in HU samples vs CON ($p = 0.001$) (**Figure 3.9**). Losartan partially prevented the rise in concentration of sarcolemma-localized Nox2 subunits, with each of the measured subunits remaining non-significantly different from CON and CONL groups.

Due to our findings that unloading results in increased protein content of sarcolemma-localized Nox2 subunits, and the implication of elevated Nox2 activity, we then investigated whether this translated to elevated Nox2 activity. NADPH-dependent superoxide production was measured by lucigenin chemiluminescence in soleus muscle homogenates. Using NADPH as a substrate, superoxide was significantly increased by 38.4% in HU muscles compared to CON ($p = 0.0282$) (**Figure 3.10**). In an effort to establish that NADPH oxidase was the main source of NADPH-dependent superoxide production in the HU soleus muscles, we used inhibitors of NADPH oxidase and a potent superoxide mimetic (EUK134). Treatment with 50 µM of EUK134 resulted in an almost complete abolishment of superoxide production. The general NADPH oxidase inhibitor DPI prevented approximately an 80% reduction of superoxide production across the groups, strongly suggesting that the superoxide produced was primarily due to

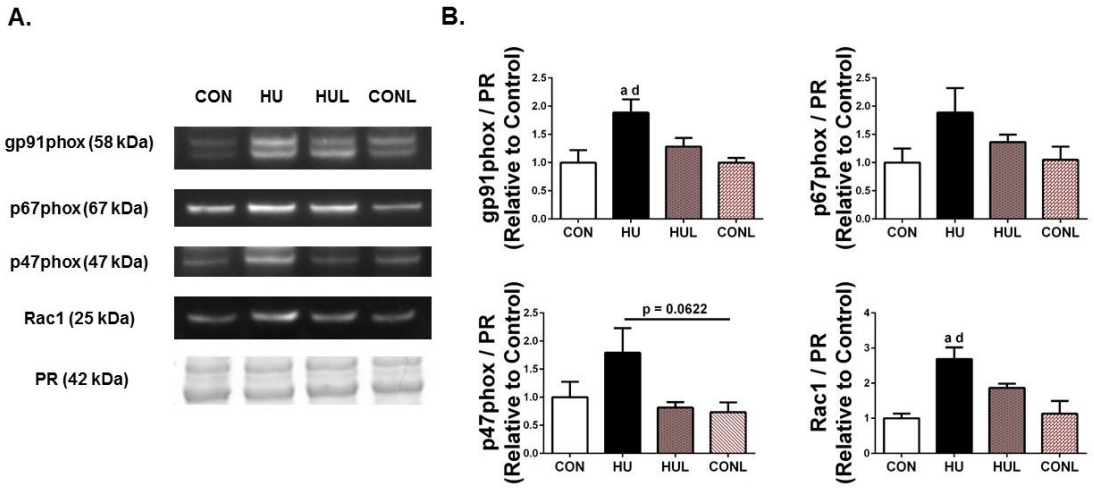

Figure 3.9. Mechanical unloading-induced alterations in NADPH oxidase isoform 2 (Nox2) protein content in the membrane fraction of soleus muscles. ***A,*** representative western blot detection of select Nox2 subunits in the soleus muscle membrane fraction. ***B,*** quantification of Nox2 western blot detection. Ponceau S Red (PR) stain (~42 kDa mark) used as a loading control for western blotting quantification. Values are presented as fold control of mean ± SEM. Values sharing the same letter are not significantly different ($p < 0.05$): [a] indicates different from CON; [c] indicates different from HUL; [d] indicates different from CONL.

NADPH oxidases. Use of the Nox2 specific pharmacological inhibitor gp91dstat resulted in more than a 50% reduction in superoxide production, suggesting Nox2 as a major Nox complex contributing to NADPH-dependent superoxide production.

3.3.3 Dislocation of Sarcolemmal nNOSμ Driven by Prolonged Mechanical Unloading is Mitigated by AT1R Blockade.

In the next set of experiments, we tested the hypothesis that hindlimb unloading-induced dislocation of nNOSμ from the sarcolemma would be protected by AT1R blockade. Localization of nNOSμ protein was assessed by immunofluorescence staining which revealed a substantial reduction in sarcolemma-localized nNOSμ in HU soleus

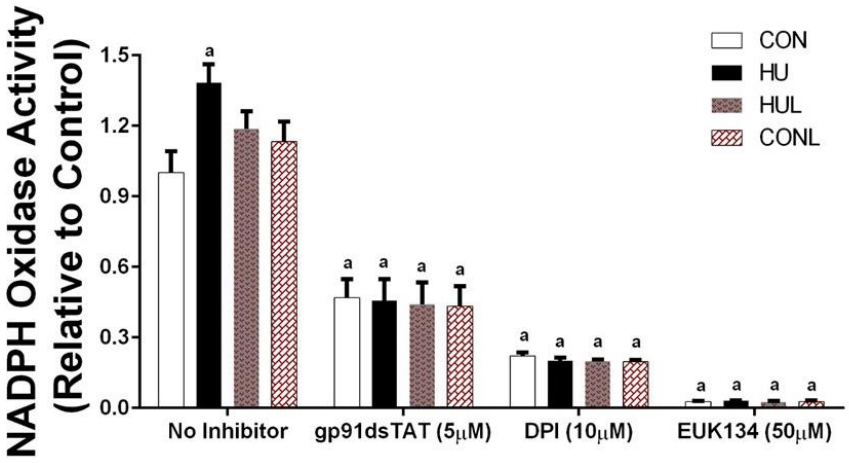

Figure 3.10. AT1R blockade ameliorates NADPH oxidase superoxide production in soleus muscles from hindlimb unloaded rats. NADPH-dependent superoxide production was assessed by lucigenin chemiluminscence. Soleus muscles were pooled for each group (2 pools per group; n = 3 muscles per pooled sample). Comparison of superoxide production in the absence and presence of ROS inhibitors: EUK-134 (50 μM), an SOD/Catalase mimetic; diphenyleneiodonium (DPI; 10 μM), a non-specific NADPH oxidase inhibitor; and gp91ds-tat (5 μM), a NADPH oxidase isoform 2 specific inhibitor. Superoxide production was compared to the level of control without an inhibitor. Values are presented as fold control of mean ± SEM. Values sharing the same letter are not significantly different ($p < 0.05$): [a] indicates different from CON; [c] indicates different from HUL; [d] indicates different from CONL.

muscle fibers, an effect that appeared to be partially prevented by treatment with losartan (**Figure 3.11A**). To confirm the immunofluorescence observations, we performed subcellular fractionation and western blotting to detect membrane-localized and cytoplasmic localized nNOS protein (**Figure 3.11B & C**). HU muscles were found to have 52.9% less sarcolemma-localized nNOSμ than CON ($p < 0.0001$), whereas HUL muscles contained only 26.5% less, although still significantly lower than CON and CONL ($p = 0.0121$ and 0.0032, respectively) (**Figure 3.11B**). While cytoplasmic nNOS was not found to be different across groups, there was a 30% increase in cytoplasmic

nNOS in both the HU and HUL groups compared to CON, and a 20% increase in CONL compared to CON (**Figure 3.11C**). The ratio of cytoplasmic:membrane nNOS was significantly elevated in the HU group compared to CON ($p = 0.0029$), whereas the ratio in HUL soleus was not found to be significantly different from CON or CONL (**Figure 3.11D**).

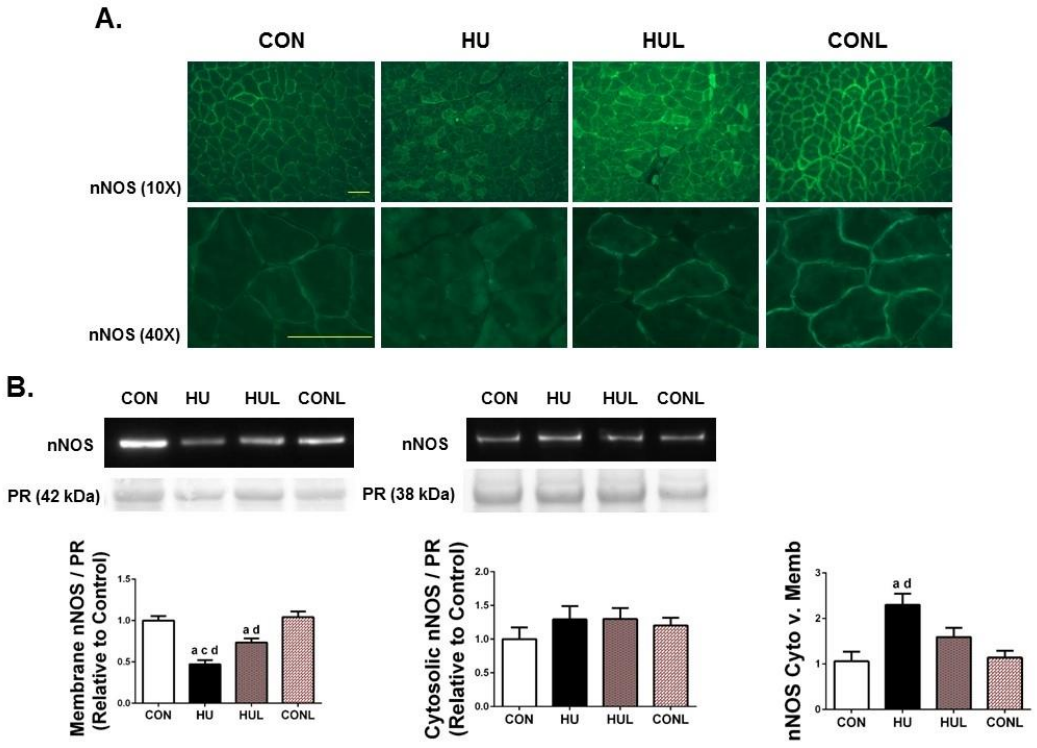

Figure 3.11. Unloading-induced reduction of sarcolemmal neuronal nitric oxide synthase (nNOS) content in soleus muscle fibers is mitigated by losartan treatment. ***A (top row),*** representative immunofluorescent images of nNOS stained soleus muscle sections. Scale bar = 100 µm. ***B,*** western blot detection of nNOS protein content in the membrane fraction. ***C,*** detection of nNOS protein content in the cytosolic fraction. ***D,*** ratio of cytosolic nNOS content to membrane content of nNOS based subcellular fractionation and western blot data. Ponceau S Red (PR) stain (~42 kDa mark for membrane fraction; ~38 kDa mark for cytosolic fraction) used as a loading control for western blotting quantification. Values are presented as fold control of mean ± SEM. Values sharing the same letter are not significantly different ($p < 0.05$): [a] indicates different from CON; [c] indicates different from HUL; [d] indicates different from CONL.

Next we examined whether or not the displacement and reduction of sarcolemma nNOSμ extended towards an alteration in nNOS-produced •NO. Soleus muscle cross-sections were subjected to NADPH-diaphorase staining to determine the localization of active •NO in muscle fibers, as seen in **Figure 3.12A**. Visually, apparent differences in sarcolemma nNOSμ activity were easily noticeable between CON and HU. Determination of the percentage of NADPH diaphorase-positive staining along the sarcolemma revealed a similar decrement in nNOSμ activity in HU vs CON ($p < 0.0001$) (**Figure 3.12B**) as that found in the nNOSμ membrane localization experiments (Figure 3.11). Interestingly, losartan administration during HU maintained sarcolemma-associated nNOSμ activity near control levels (49% vs 52.96%; $p = 0.6897$), which was dramatically higher than HU ($p < 0.0001$) (**Figure 3.12B**).

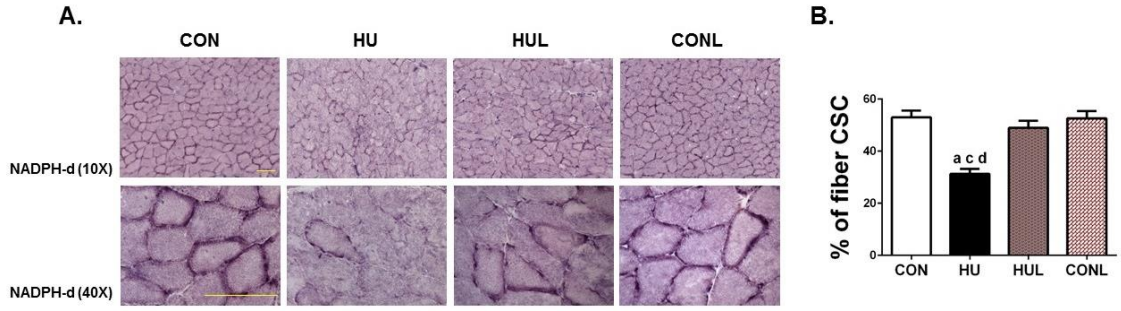

Figure 3.12. Unloading-induced reduction of active sarcolemmal nNOS in soleus muscle fibers is mitigated by losartan treatment. ***A (top row),*** representative images of soleus muscle sections subjected to NADPH-diaphorase (NADPH-dia) histochemical assay to detect sarcolemmal nNOS activity taken at 10x magnification; ***(bottom row),*** NADPH-dia images taken at 40x magnification. Scale bar = 100 μm. ***B,*** quantification of NADPH-dia reactive staining found at the sarcolemma. Presented as percentage of cross-sectional circumference (CSC) that is stained positive. Values are means ± SEM. Values sharing the same letter are not significantly different ($p < 0.05$): [a] indicates different from CON; [c] indicates different from HUL; [d] indicates different from CONL.

3.3.4 AT1R Blockade Significantly Lessens the Unloading-Induced Nuclear Accumulation of FoxO3a.

Important regulators of skeletal muscle atrophy with disuse include FoxO3a and p53 transcription factors. Our lab and others have previously shown that dephosphorylation and activation of FoxO3a was dependent on nNOSμ dislocation from the sarcolemma (Suzuki *et al.*, 2007; Lawler *et al.*, 2014). Given that losartan mitigated nNOSμ translocation and alterations in sarcolemmal nNOSμ activity, we tested the hypothesis that losartan would lead to a reduction in nuclear FoxO3a. Co-localization of positively stained FoxO3a myonuclei with DAPI demonstrated a dramatic rise (> 50%) in nuclear-localized FoxO3a in HU soleus vs CON ($p < 0.0001$) (**Figure 3.13A & B**). This effect was ameliorated in HUL muscles with only a 20% increase vs CON, and 45% lower than HU ($p < 0.0001$). However, HUL still contained a significantly greater amount of positively stained FoxO3a nuclei compared to CON and CONL ($p = 0.6897$ and 0.742, respectively). Further confirmation of hindlimb unloading-induced nuclear translocation of FoxO3a was observed with western blotting of the nuclear fraction (**Figure 3.13C**). HU displayed a drastic 770% increase in FoxO3a nuclear content compared to CON ($p = 0.0003$). HUL remained 655% lower than HU in FoxO3a nuclear content ($p = 0.0019$). Blot data did not find a significant elevation in FoxO3a nuclear content between HUL, CON and CONL.

In addition to FoxO3a, p53 has been found at increased concentrations and activity levels as a transcription factor during the early stages of disuse (Fox *et al.*, 2014). We probed the nuclear fraction of soleus muscles to assess p53 content. Similar

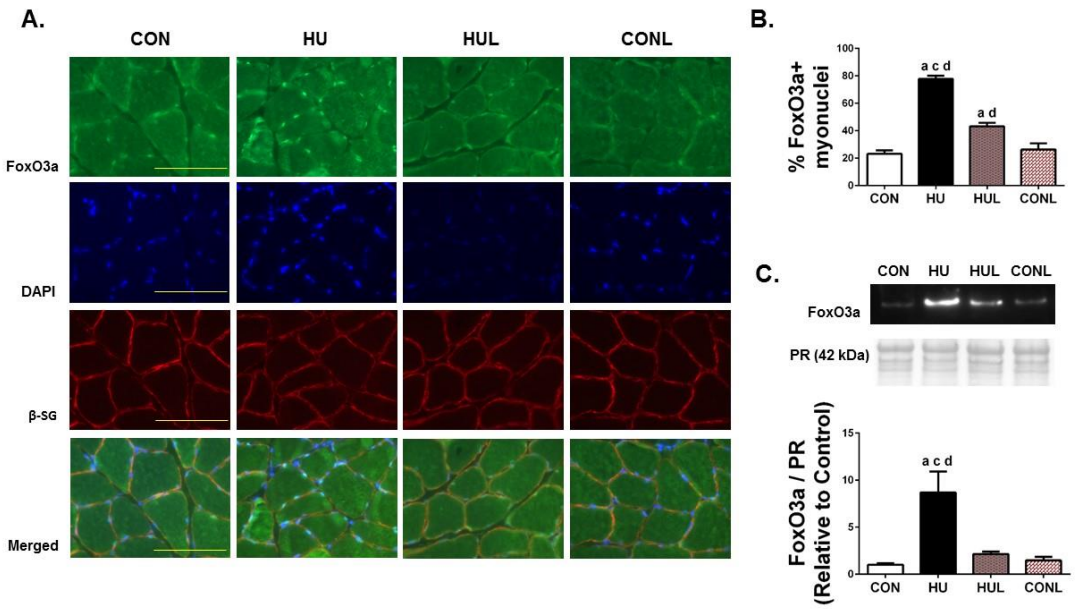

Figure 3.13. Nuclear localization of FoxO3a due to hindlimb unloading disuse is partially prevented by losartan administration. ***A,*** soleus muscle cross-sections stained with ***(top row)*** FoxO3a, ***(second row)*** DAPI, ***(third row)*** beta-sarcoglycan (b-SG), and the ***bottom row*** is comprised of the merged images. Scale bar = 100 µm. ***B,*** graphical representation of the percentage myonuclei positively stained for FoxO3a. Values are means ± SEM. ***C,*** detection of FoxO3a via western blotting in the nuclear fraction. Ponceau S Red (PR) stain (~42 kDa mark) used as a loading control for western blotting quantification. Values are presented as fold control of mean ± SEM. Values sharing the same letter are not significantly different ($p < 0.05$): [a] indicates different from CON; [c] indicates different from HUL; [d] indicates different from CONL.

to the hindlimb unloading-induced increase in FoxO3a nuclear content, we observed a significant 310% increase in HU p53 nuclear content compared to CON ($p < 0.0001$) (**Figure 3.14**). In contrast to the FoxO3a nuclear content, HUL muscles were found to have a significant elevation of nuclear p53 compared to CON and CONL ($p = 0.0003$ and $p < 0.0001$, respectively). These data indicate that losartan may be interfering with select atrophy pathways with mechanical unloading, independent of p53 signaling.

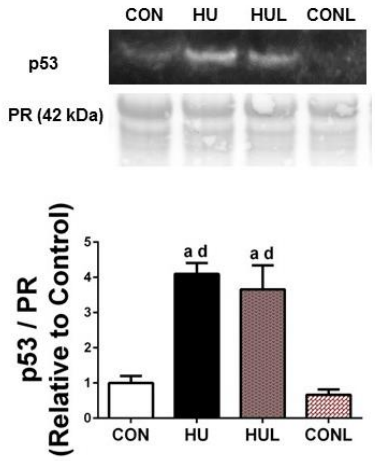

Figure 3.14. Nuclear content of the atrophy-inducing transcription factor p53 is dramatically increased following 7 days of hindlimb unloading, even in losartan-treated animals. ***A,*** western blot detection of p53 in the nuclear fraction of soleus muscles. Ponceau S Red (PR) stain (~42 kDa mark) used as a loading control for western blotting quantification. Values are presented as fold control of mean ± SEM. Values sharing the same letter are not significantly different ($p < 0.05$): [a] indicates different from CON; [c] indicates different from HUL; [d] indicates different from CONL.

3.4 Discussion

In this study, administration of the angiotensin II type 1 receptor (AT1R) blocker losartan during hindlimb unloading attenuated the disuse-induced phenotypic alterations including reductions in soleus muscle fiber CSA and the slow-twitch to fast-twitch fiber type shift. These effects were due in part to abrogation of the mechanical unloading-induced rise in ROS levels and the accumulation and activation of Nox2. In addition, losartan treatment during unloading was associated with a significant protection against the unloading-induced dislocation of nNOS from the sarcolemma. Furthermore, losartan treatment also significantly reduced the nuclear accumulation of the atrophy-associated transcription factor FoxO3a, which has been observed to be regulated in part by

displaced nNOSμ. In the following paragraphs we provide a discussion of the principle findings.

3.4.1 Renin Angiotensin System (RAS) and Hindlimb Unloading-Induced Atrophy

Elevated AngII levels cause skeletal muscle wasting, and the use of angiotensin converting enzyme (ACE) inhibitors and / or AT1R antagonists have proven effective against muscle wasting (Sukhanov *et al.*, 2011; Cabello-Verrugio *et al.*, 2012a). For instance, AT1R blockade using losartan ameliorated the exacerbation of disuse atrophy in sarcopenic mouse muscle (Burks *et al.*, 2011). In addition, a recent report found that treatment with the AngII antagonistic renin-angiotensin system peptide, Ang-(1-7), offered significant protection against atrophy due to limb immobilization (Morales *et al.*, 2016). However, there is little evidence concerning circulating AngII levels during disuse. In the mechanical ventilation model of disuse, Kwon et. al (2015) reported a significant rise in plasma AngII after 12 hours of ventilation (Kwon *et al.*, 2015). Moreover, in the hindlimb unloading model, plasma AngII levels are significantly increased and peak at 7 days before returning to baseline levels (Chung *et al.*, 2012). Other than inhibiting AngII – AT1R binding, losartan may be exerting protective effects as a byproduct of AT1R antagonism which leads to an increase in circulating levels of Ang-(1-7) (Schindler *et al.*, 2007). In skeletal muscle, Ang-(1-7) will bind to the Mas receptor and promote Akt activation, thereby inhibiting UPP signaling (Cisternas *et al.*, 2015; Morales *et al.*, 2016). Interestingly, evidence indicates that ligands other than AngII can activate AT1R signaling (Zou *et al.*, 2004); however the identity of those ligands still remain unknown.

3.4.2 AT1R Blockade Mitigated the Disuse-Induced Morphological Changes.

Losartan treatment has previously been shown to prevent the reduction in myofiber CSA following 21 days of limb immobilization via stapling in aged mice (Burks *et al.*, 2011). Furthermore, Ang-(1-7), a downstream fragment of AngII via ACE2 (angiotensin converting enzyme II), reportedly inhibits casting-induced reductions of fiber CSA in the tibialis anterior following 2 weeks of immobilization by way of signaling through the G-protein Mas receptor (Morales *et al.*, 2016). Our findings indicate that hindlimb unloading-induced muscle fiber atrophy (**Figure 3.5**) and fiber-type shift (**Figure 3.6**) were limited by daily administration of losartan following one week of unloading. Interestingly, we found losartan treatment during unloading prevented atrophy of Type I but not Type II fibers. To our knowledge, demonstration of a fiber type-specific expression pattern of AT1R has not been shown, and future studies will need to address this issue. While losartan administration offered partial protection against the unloading-induced decrease in muscle fiber CSA and fiber type shift, it did not protect against loss of soleus mass (**Table 3.1**). This finding may be explained in part by the impact of AT1R blockade on the prevention of extra-myocyte build-up in the soleus muscle, as shown in **Figure 3.7.** In support of this observation, AT1R antagonism using losartan ameliorates skeletal muscle fibrosis and extra-myofiber accumulation due to disuse, injury, (Burks *et al.*, 2011) and CTGF overexpression (Cabello-Verrugio *et al.*, 2012b). Altogether, daily losartan treatment during unloading helped mitigate the reduction in Type I fiber CSA, fiber type shift, and the accumulation of extra-myocyte

tissue, thus favoring a healthier, more functional muscle phenotype, even though total soleus mass was still reduced.

3.4.3 Hindlimb Unloading-Associated Rise in ROS is Partially Prevented by Daily Losartan Treatment.

Data presented here is consistent with theories suggesting the importance of elevated ROS during disuse atrophy. We observed an unloading-induced rise in superoxide as assessed by ethidium-positive nuclei in soleus muscle cross-sections (**Figure 3.8**). Additionally, we found increased superoxide production in a lucigenin chemiluminescence assay when NADPH was presented as a substrate in tissue homogenates (**Figure 3.10**). Using general and specific inhibitors, our data indicate that a major source of superoxide when NADPH was present was NADPH oxidase (**Figure 3.10**). Moreover, we observed unloading-induced increases in sarcolemma content of NADPH oxidase isoform 2 (**Figure 3.9**). Increased content of the membrane-bound subunit gp91phox indicates elevated expression of this subunit, while increased abundance of sarcolemma-localized cytoplasmic subunits (i.e., p67phox, p47phox, and rac-1) suggest increased activity of the complex (**Figure 3.9**). Skeletal muscle Nox activity has become predominately known for its actions in response to contractile activity in healthy (Pearson *et al.*, 2014) as well as dystrophic muscle (Whitehead *et al.*, 2010). However, elevated expression of Nox2 subunits and Nox activity has also been observed in plantaris muscle atrophy in response to myocardial infarction (Bechara *et al.*, 2014), implicating a role for Nox complexes and Nox2 in muscle atrophy. Moreover, our current findings along with our previous observations (Lawler *et al.*, 2014) indicate

that hindlimb unloading can lead to increased expression and activation of sarcolemma-localized Nox2 subunits. In connection with those findings, Bhattacharya et al. (2014) observed increased Nox activity in gastrocnemius muscles from denervated mice (Bhattacharya *et al.*, 2014). Together, these data indicate that Nox2 and Nox-derived superoxide are responsive not only to activity (i.e., skeletal muscle contraction) but also to prolonged periods of inactivity (i.e., disuse) and the general atrophic process.

Our current observation that administration of the AT1R blocker losartan reduced the unloading-induced increase in superoxide and Nox2 subunits (**Figures 3.8 – 3.10**) is in agreement with findings from previous studies. While the AT1R – Nox connection has been shown previously in a variety of tissues, including skeletal muscle (Sukhanov *et al.*, 2011), we are the first to report this connection during disuse atrophy. For example, L6 myotubes treated with AngII displayed increased Nox activity and subsequent ROS production, effects that were mitigated by the Nox inhibitor, apocynin and the AT1R antagonist, losartan (Wei *et al.*, 2006). Furthermore, elevated ROS levels in skeletal muscle were detected in rats treated with AngII, an effect that coincided with an up-regulation of gp91phox (Zhao *et al.*, 2006). In relation to skeletal muscle wasting, Semprun-Prieto et al. (2011) observed that AngII-induced atrophy was associated with elevated superoxide production, with both ROS production and atrophy prevented in p47phox$^{-/-}$ mice (Semprun-Prieto *et al.*, 2011). Additional evidence shows increased mitochondrial ROS (Tabony *et al.*, 2011) and mitochondrial dysfunction (Kadoguchi *et al.*, 2015) following AngII administration. Interestingly, Tabony et al. (2011) found that inhibition of mitochondrial-derived ROS did not alter the degree of AngII-induced

skeletal muscle wasting (Tabony *et al.*, 2011), indicating that AngII atrophy signaling is likely through Nox rather than mitochondrial ROS production.

3.4.4 Dislocation of nNOSμ Caused by Disuse is Limited by Daily Losartan Treatment.

Prolonged periods of disuse have been shown to result in the sarcolemma dislocation of the mu isoform of neuronal nitric oxide synthase (nNOSμ) (Suzuki *et al.*, 2007; Llano-Diez *et al.*, 2012; Sandona *et al.*, 2012; Lawler *et al.*, 2014). Whether or not disuse leads to a reduction in nNOSμ expression remains controversial (Suzuki *et al.*, 2007; Lomonosova *et al.*, 2011). We have previously reported that 54 hours of hindlimb unloading leads to nNOSμ translocation, coinciding with a rise in sarcolemma-associated oxidative modifications, suggesting that elevated ROS is a causal event in nNOSμ translocation (Lawler *et al.*, 2014). As expected, in the current study we observed that 7 days of hindlimb unloading was associated with dislocation of nNOSμ determined via immunofluorescence of soleus muscle cross-sections and western blotting following subcellular fractionation (**Figure 3.11**). Interestingly, losartan treatment throughout the unloading period offered partial protection against the unloading-induced nNOSμ alterations (**Figure 3.11**). While western blot detection of sarcolemmal nNOSμ found that HUL rats still had significantly less membrane-associated nNOSμ, through NADPH-diaphorase histochemical staining to assess nNOS activity, HUL solei were shown to have sarcolemma nNOS activity similar to controls (**Figure 3.12**).

Intriguing findings indicate that NOS and the resultant nitric oxide (•NO) are involved in the regulation of type I myosin heavy chain expression (Sellman *et al.*, 2006;

Suwa *et al.*, 2015). For example, a significant reduction in the percentage of type I fibers and concomitant increase in type IIa fibers were found in the rat soleus following 8 weeks of NOS inhibition (Suwa *et al.*, 2015). Prolonged periods of disuse are known to be associated with a type I to type II shift in fiber type, as we have shown here, and unloading nNOSμ alterations may be playing a critical role in the phenotype adaptation. In support of this notion, we found that losartan offered protection against unloading-induced nNOSμ localization and activity alterations accompanied by protection against the shift in fiber type.

3.4.5 Atrophy-Related Transcription Factors are Elevated with Hindlimb Unloading.

Unloading-induced nNOSμ dislocation has also been associated with dephosphorylation of FoxO3a (Suzuki *et al.*, 2007; Lawler *et al.*, 2014), thus leading to shuttling of FoxO3a to the nucleus where it acts as a transcription factor for key atrogenes: MuRF1 and MAFbx/Atrogin 1 (Suzuki *et al.*, 2007). Disuse atrophy is primarily driven by the upregulation of E3 ubiquitin ligases MuRF-1 and MAFbx/Atrogin-1 (Bodine *et al.*, 2001). Expression of these two ligases is promoted by FoxO3a (Schiaffino *et al.*, 2013). Activation of FoxO3a is directed by inhibition of Akt (Schiaffino *et al.*, 2013) and has been shown to be sensitive to sarcoplasmic nNOS derived •NO (Suzuki *et al.*, 2007). We found consistent elevation of nuclear FoxO3a, detected by both DAPI-localized immunofluorescence and nuclear fraction abundance with HU (**Figure 3.13**). Losartan indeed abrogated upregulation of nuclear FoxO3a and thus nuclear translocation and activation (**Figure 3.13**). This suggests that AT1R – Nox2 signaling is important in activation of FoxO3a. Elevated levels of dephosphorylated

FoxO1 and FoxO3a proteins, as well as the associated transcription of the E3 ligases MuRF1 and MAFbx/Atrogin 1, have been observed in AngII treated mice (Tabony *et al.*, 2011; Tabony *et al.*, 2014). Our findings suggest that AT1R may be upstream of an atrophic pathway involving Nox2, ROS, nNOSμ dislocation and FoxO3a activation during mechanical unloading.

In addition to the transcription factor actions of FoxO3a during disuse, recent research has implicated the tumor suppressor p53 in the early stages of disuse atrophy. For instance, p53 protein content has been reported to be significantly higher in the soleus muscle during hindlimb unloading within the first 6 hours of disuse (Ferreira *et al.*, 2008). Furthermore, p53 is significantly elevated with 3 days of disuse (Fox *et al.*, 2014), but whether this occurrence lasts beyond 3 days remains unknown. Here, we have shown that p53 protein is significantly elevated in the nuclear fraction of soleus muscles following 7 days of unloading (**Figure 3.14**). Unlike our FoxO3a observations, the unloading-induced rise in nuclear p53 was not ameliorated by losartan treatment (**Figure 3.14**). Previous studies using cancer cells have reported that losartan had no effect (Xiao *et al.*, 2015) or even led to an increase (Gong *et al.*, 2010) in p53 expression. Interestingly, active p53 has been associated with promoting local renin-angiotensin system (RAS) activity in cardiac myocytes in response to stretch (Leri *et al.*, 1998). Local RAS signaling has also been observed in C2C12 skeletal muscle cells in response to stretch (Johnston *et al.*, 2011), but the authors did not examine p53 involvement. Whether p53 enhances local RAS signaling *in vivo* or in response to disuse in skeletal muscle remains unknown. Given that p53 was upstream and suppressed spermine

oxidase (Bongers *et al.*, 2015), it is possible that p53 acts upon a metabolic pathway contributing to disuse atrophy, and AT1R – Nox2 signaling may be integrated into an independent mechanotransductive pathway.

CHAPTER IV

SUMMARY AND CONCLUSIONS

4.1 Summary and Conclusions

As discussed in Chapter II, elevated ROS during disuse can lead to a stressful environment in skeletal muscle fibers, resulting in decreased rates of protein synthesis and increased rates of degradation. Currently, the field of disuse atrophy research lacks a complete understanding of the specific upstream signaling events triggering the various sources of ROS. In addition, the specific regulatory actions downstream of the rise in levels of ROS, such as the mechanistic events leading to the untethering of sarcolemmal nNOSμ and activation of pro-atrophic transcription factors, are still an enigma.

In Chapter III we presented findings demonstrating that AT1R blockade during 7 days of hindlimb unloading mitigates the extent of hindlimb unloading-induced soleus muscle atrophy (*summarized in* **Figure 4.1**). Indeed, disuse-induced reductions in fiber CSA, shift in fiber type, and connective tissue accumulation were limited by daily losartan administration. Additionally, disuse-associated elevations in ROS were attenuated by losartan treatment, which was in part due to a reduction in content and activity of NADPH oxidase 2 (Nox2). Furthermore, nNOSμ dislocation from the sarcolemma to the sarcoplasm due to prolonged disuse was partially prevented by losartan, as was the reduction in sarcolemmal nNOSμ activity. Finally, antagonism of AT1R during unloading ameliorated the rise in nuclear content of FoxO3a but not p53.

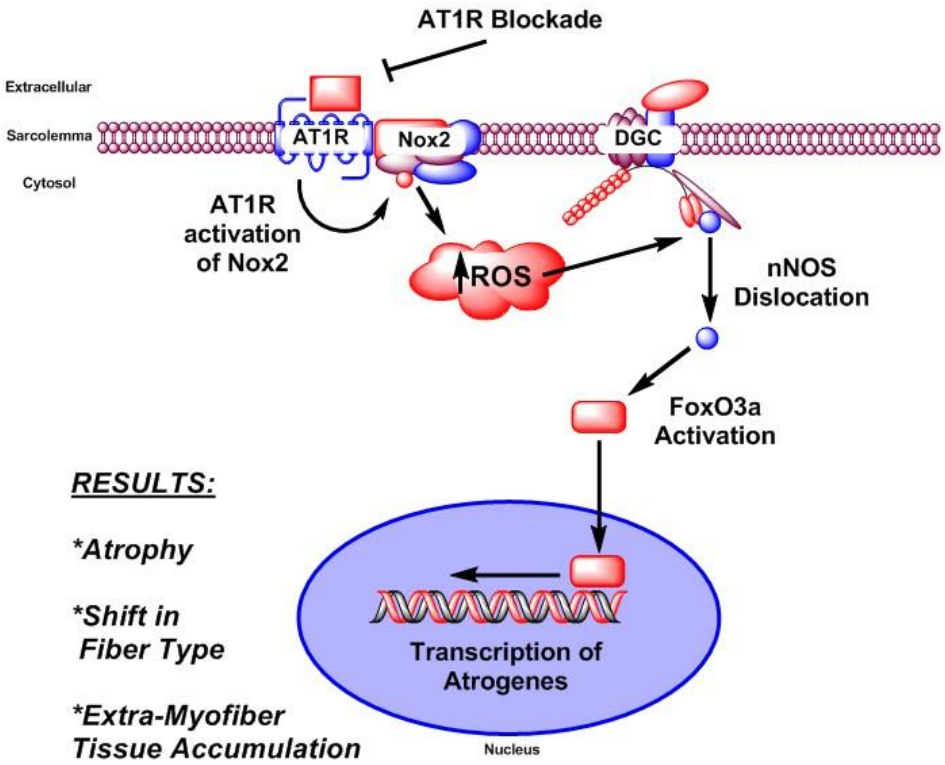

Figure 4.1. Model of the influence of AT1R activation during hindlimb unloading-induced atrophy.

Our experiments from Chapter III reveal discoveries that are integral towards the unraveling of upstream factors promoting ROS production during hindlimb unloading atrophy. Activation of AT1R appears to be a critical step in stimulating Nox2 activity and accumulation during mechanical unloading. Refer to **Figure 4.2** for an illustration of how the current findings fit into the scheme of disuse ROS-associated events.

4.2 Clinical Relevance

Preventing, limiting, or delaying disuse muscle atrophy is a critical biomedical issue with application to spaceflight, casting, bed rest, orthopedic injuries, denervation

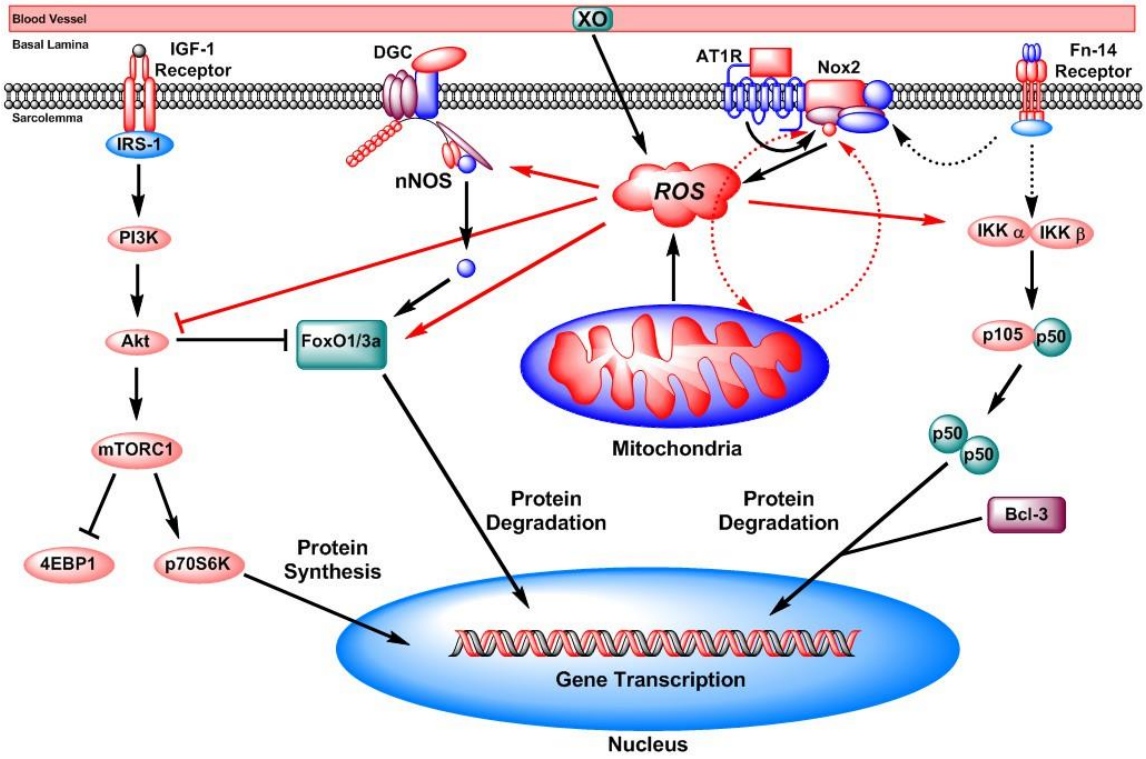

Figure 4.2. Updated version of Figure 2.2. The findings gleaned from the study presented in Chapter III where we observed the involvement of AT1R activation in the regulation of Nox2-ROS production are now added to an illustration depicting critical signaling pathways controlling muscle fiber size during disuse-induced atrophy and the regulatory schemes exerted by ROS. The combination of reactive oxygen species (ROS) derived from mitochondria, NADPH oxidase isoform 2 (Nox2), and xanthine oxidase (XO) results in an increased ROS concentration in myofibers during periods of disuse. Elevated ROS can blunt Akt-mTORC1 protein synthesis signaling, induce dislocation of nNOS from the DGC towards the sarcoplasm, enhance dephosphorylation of FoxO1/3a, and promote NFkB signaling. In addition, ROS from Nox2 and/or mitochondria may promote a ROS-induced ROS-release amplification scheme (as shown by the dashed red-lines with arrowheads). ROS regulatory functions are shown with red lines. Dashed lines indicate hypotheses concerning signaling events made by the authors based on published research findings. This is a simplified figure illustrating ROS-regulation of disuse fiber atrophy, refer to text for brief discussions on alternative pro-degradation routes (e.g. calpains, caspase-3, autophagy-lysosomal).

and other effectors of skeletal muscle disuse. To our knowledge, our study presented in Chapter III is the first to examine the effectiveness of losartan treatment on disuse

atrophy with administration starting less than one week prior to the onset of disuse. Still unknown is whether losartan would be capable of offering protective effects if administration began after the onset of disuse, which would be an important discovery since many instances of forced bed rest, limb casting, etc., are unplanned events. Notably, data presented here further supports the effectiveness of AT1R blockade in limiting or possibly delaying disuse atrophy, providing additional rationale for the usage of a cost-effective and FDA-approved pharmaceutical agent (losartan) during prolonged periods of disuse.

REFERENCES

Abrigo J, Rivera JC, Simon F, Cabrera D & Cabello-Verrugio C. (2016). Transforming growth factor type beta (TGF-beta) requires reactive oxygen species to induce skeletal muscle atrophy. *Cell Signal* **28,** 366-376.

Adams V, Yu J, Mobius-Winkler S, Linke A, Weigl C, Hilbrich L, Schuler G & Hambrecht R. (1997). Increased inducible nitric oxide synthase in skeletal muscle biopsies from patients with chronic heart failure. *Biochem Mol Med* **61,** 152-160.

Allen DL, Linderman JK, Roy RR, Grindeland RE, Mukku V & Edgerton VR. (1997). Growth hormone/IGF-I and/or resistive exercise maintains myonuclear number in hindlimb unweighted muscles. *J Appl Physiol (1985)* **83,** 1857-1861.

Arbogast S, Smith J, Matuszczak Y, Hardin BJ, Moylan JS, Smith JD, Ware J, Kennedy AR & Reid MB. (2007). Bowman-Birk inhibitor concentrate prevents atrophy, weakness, and oxidative stress in soleus muscle of hindlimb-unloaded mice. *J Appl Physiol (1985)* **102,** 956-964.

Balakumar P & Jagadeesh G. (2014). A century old renin-angiotensin system still grows with endless possibilities: AT1 receptor signaling cascades in cardiovascular physiopathology. *Cell Signal* **26,** 2147-2160.

Batt J, Bain J, Goncalves J, Michalski B, Plant P, Fahnestock M & Woodgett J. (2006). Differential gene expression profiling of short and long term denervated muscle. *FASEB J* **20,** 115-117.

Bechara LR, Moreira JB, Jannig PR, Voltarelli VA, Dourado PM, Vasconcelos AR, Scavone C, Ramires PR & Brum PC. (2014). NADPH oxidase hyperactivity induces plantaris atrophy in heart failure rats. *Int J Cardiol* **175,** 499-507.

Betters JL, Criswell DS, Shanely RA, Van Gammeren D, Falk D, Deruisseau KC, Deering M, Yimlamai T & Powers SK. (2004). Trolox attenuates mechanical ventilation-induced diaphragmatic dysfunction and proteolysis. *Am J Respir Crit Care Med* **170,** 1179-1184.

Bhattacharya A, Hamilton R, Jernigan A, Zhang Y, Sabia M, Rahman MM, Li Y, Wei R, Chaudhuri A & Van Remmen H. (2014). Genetic ablation of 12/15-lipoxygenase but not 5-lipoxygenase protects against denervation-induced muscle atrophy. *Free Radic Biol Med* **67,** 30-40.

Bodine SC & Baehr LM. (2014). Skeletal muscle atrophy and the E3 ubiquitin ligases MuRF1 and MAFbx/atrogin-1. *Am J Physiol Endocrinol Metab* **307,** E469-484.

Bodine SC, Latres E, Baumhueter S, Lai VK, Nunez L, Clarke BA, Poueymirou WT, Panaro FJ, Na E, Dharmarajan K, Pan ZQ, Valenzuela DM, DeChiara TM, Stitt TN, Yancopoulos GD & Glass DJ. (2001). Identification of ubiquitin ligases required for skeletal muscle atrophy. *Science* **294,** 1704-1708.

Bongers KS, Fox DK, Kunkel SD, Stebounova LV, Murry DJ, Pufall MA, Ebert SM, Dyle MC, Bullard SA, Dierdorff JM & Adams CM. (2015). Spermine oxidase maintains basal skeletal muscle gene expression and fiber size and is strongly repressed by conditions that cause skeletal muscle atrophy. *Am J Physiol Endocrinol Metab* **308,** E144-158.

Brenman JE, Chao DS, Xia H, Aldape K & Bredt DS. (1995). Nitric oxide synthase complexed with dystrophin and absent from skeletal muscle sarcolemma in Duchenne muscular dystrophy. *Cell* **82,** 743-752.

Brunet A, Bonni A, Zigmond MJ, Lin MZ, Juo P, Hu LS, Anderson MJ, Arden KC, Blenis J & Greenberg ME. (1999). Akt promotes cell survival by phosphorylating and inhibiting a Forkhead transcription factor. *Cell* **96,** 857-868.

Burks TN, Andres-Mateos E, Marx R, Mejias R, Van Erp C, Simmers JL, Walston JD, Ward CW & Cohn RD. (2011). Losartan restores skeletal muscle remodeling and protects against disuse atrophy in sarcopenia. *Sci Transl Med* **3,** 82ra37.

Cabello-Verrugio C, Cordova G & Salas JD. (2012a). Angiotensin II: role in skeletal muscle atrophy. *Curr Protein Pept Sci* **13,** 560-569.

Cabello-Verrugio C, Morales MG, Cabrera D, Vio CP & Brandan E. (2012b). Angiotensin II receptor type 1 blockade decreases CTGF/CCN2-mediated damage and fibrosis in normal and dystrophic skeletal muscles. *J Cell Mol Med* **16,** 752-764.

Chen YW, Gregory CM, Scarborough MT, Shi R, Walter GA & Vandenborne K. (2007). Transcriptional pathways associated with skeletal muscle disuse atrophy in humans. *Physiol Genomics* **31,** 510-520.

Chung SY, Kim SK, Hong CW, Oh KW, Kim KT, Sul JG, Chung JW & Kwon MS. (2012). The time-dependent alteration of anti-diuretic hormone system in hindlimb unloaded rats. *J Physiol Pharmacol* **63,** 87-94.

Cisternas F, Morales MG, Meneses C, Simon F, Brandan E, Abrigo J, Vazquez Y & Cabello-Verrugio C. (2015). Angiotensin-(1-7) decreases skeletal muscle atrophy induced by angiotensin II through a Mas receptor-dependent mechanism. *Clin Sci (Lond)* **128,** 307-319.

Cohn RD, van Erp C, Habashi JP, Soleimani AA, Klein EC, Lisi MT, Gamradt M, ap Rhys CM, Holm TM, Loeys BL, Ramirez F, Judge DP, Ward CW & Dietz HC. (2007). Angiotensin II type 1 receptor blockade attenuates TGF-beta-induced failure of muscle regeneration in multiple myopathic states. *Nat Med* **13,** 204-210.

Csanyi G, Cifuentes-Pagano E, Al Ghouleh I, Ranayhossaini DJ, Egana L, Lopes LR, Jackson HM, Kelley EE & Pagano PJ. (2011). Nox2 B-loop peptide, Nox2ds, specifically inhibits the NADPH oxidase Nox2. *Free Radic Biol Med* **51,** 1116-1125.

Daiber A. (2010). Redox signaling (cross-talk) from and to mitochondria involves mitochondrial pores and reactive oxygen species. *Biochim Biophys Acta* **1797,** 897-906.

de Boer MD, Selby A, Atherton P, Smith K, Seynnes OR, Maganaris CN, Maffulli N, Movin T, Narici MV & Rennie MJ. (2007). The temporal responses of protein synthesis, gene expression and cell signalling in human quadriceps muscle and patellar tendon to disuse. *J Physiol* **585,** 241-251.

Derbre F, Ferrando B, Gomez-Cabrera MC, Sanchis-Gomar F, Martinez-Bello VE, Olaso-Gonzalez G, Diaz A, Gratas-Delamarche A, Cerda M & Vina J. (2012). Inhibition of xanthine oxidase by allopurinol prevents skeletal muscle atrophy: role of p38 MAPKinase and E3 ubiquitin ligases. *PLoS One* **7,** e46668.

Dimauro I, Pearson T, Caporossi D & Jackson MJ. (2012). A simple protocol for the subcellular fractionation of skeletal muscle cells and tissue. *BMC Res Notes* **5,** 513.

Dupont E, Cieniewski-Bernard C, Bastide B & Stevens L. (2011). Electrostimulation during hindlimb unloading modulates PI3K-AKT downstream targets without preventing soleus atrophy and restores slow phenotype through ERK. *Am J Physiol Regul Integr Comp Physiol* **300,** R408-417.

Ebert SM, Dyle MC, Kunkel SD, Bullard SA, Bongers KS, Fox DK, Dierdorff JM, Foster ED & Adams CM. (2012). Stress-induced skeletal muscle Gadd45a expression reprograms myonuclei and causes muscle atrophy. *J Biol Chem* **287,** 27290-27301.

Egerman MA & Glass DJ. (2014). Signaling pathways controlling skeletal muscle mass. *Crit Rev Biochem Mol Biol* **49,** 59-68.

Ferrando AA, Lane HW, Stuart CA, Davis-Street J & Wolfe RR. (1996). Prolonged bed rest decreases skeletal muscle and whole body protein synthesis. *Am J Physiol* **270,** E627-633.

Ferreira R, Neuparth MJ, Vitorino R, Appell HJ, Amado F & Duarte JA. (2008). Evidences of apoptosis during the early phases of soleus muscle atrophy in hindlimb suspended mice. *Physiol Res* **57,** 601-611.

Ferreira R, Vitorino R, Neuparth MJ, Appell HJ, Duarte JA & Amado F. (2009). Proteolysis activation and proteome alterations in murine skeletal muscle submitted to 1 week of hindlimb suspension. *Eur J Appl Physiol* **107,** 553-563.

Fox DK, Ebert SM, Bongers KS, Dyle MC, Bullard SA, Dierdorff JM, Kunkel SD & Adams CM. (2014). p53 and ATF4 mediate distinct and additive pathways to skeletal muscle atrophy during limb immobilization. *Am J Physiol Endocrinol Metab* **307,** E245-261.

Globus RK & Morey-Holton E. (2016). Hindlimb unloading: rodent analog for microgravity. *J Appl Physiol (1985)* **120,** 1196-1206.

Glover EI, Yasuda N, Tarnopolsky MA, Abadi A & Phillips SM. (2010). Little change in markers of protein breakdown and oxidative stress in humans in

immobilization-induced skeletal muscle atrophy. *Appl Physiol Nutr Metab* **35,** 125-133.

Goldberg AL, Etlinger JD, Goldspink DF & Jablecki C. (1975). Mechanism of work-induced hypertrophy of skeletal muscle. *Med Sci Sports* **7,** 185-198.

Goncalves G, Zornoff LA, Ribeiro HB, Okoshi MP, Cordaro FR, Okoshi K, Padovani CR, Aragon FF & Cicogna AC. (2005). [Blockade of renin-angiotensin system attenuates cardiac remodeling in rats undergoing aortic stenosis]. *Arq Bras Cardiol* **84,** 304-308.

Gong Q, Davis M, Chipitsyna G, Yeo CJ & Arafat HA. (2010). Blocking angiotensin II Type 1 receptor triggers apoptotic cell death in human pancreatic cancer cells. *Pancreas* **39,** 581-594.

Habashi JP, Judge DP, Holm TM, Cohn RD, Loeys BL, Cooper TK, Myers L, Klein EC, Liu G, Calvi C, Podowski M, Neptune ER, Halushka MK, Bedja D, Gabrielson K, Rifkin DB, Carta L, Ramirez F, Huso DL & Dietz HC. (2006). Losartan, an AT1 antagonist, prevents aortic aneurysm in a mouse model of Marfan syndrome. *Science* **312,** 117-121.

Heymes C, Bendall JK, Ratajczak P, Cave AC, Samuel JL, Hasenfuss G & Shah AM. (2003). Increased myocardial NADPH oxidase activity in human heart failure. *J Am Coll Cardiol* **41,** 2164-2171.

Hornberger TA, Hunter RB, Kandarian SC & Esser KA. (2001). Regulation of translation factors during hindlimb unloading and denervation of skeletal muscle in rats. *Am J Physiol Cell Physiol* **281,** C179-187.

Hudson MB, Smuder AJ, Nelson WB, Wiggs MP, Shimkus KL, Fluckey JD, Szeto HH & Powers SK. (2015). Partial Support Ventilation and Mitochondrial-Targeted Antioxidants Protect against Ventilator-Induced Decreases in Diaphragm Muscle Protein Synthesis. *PLoS One* **10,** e0137693.

Hunter RB & Kandarian SC. (2004). Disruption of either the Nfkb1 or the Bcl3 gene inhibits skeletal muscle atrophy. *J Clin Invest* **114,** 1504-1511.

Hunter RB, Stevenson E, Koncarevic A, Mitchell-Felton H, Essig DA & Kandarian SC. (2002). Activation of an alternative NF-kappaB pathway in skeletal muscle during disuse atrophy. *FASEB J* **16,** 529-538.

Ikemoto M, Nikawa T, Kano M, Hirasaka K, Kitano T, Watanabe C, Tanaka R, Yamamoto T, Kamada M & Kishi K. (2002). Cysteine supplementation prevents unweighting-induced ubiquitination in association with redox regulation in rat skeletal muscle. *Biol Chem* **383,** 715-721.

Ito N, Ruegg UT, Kudo A, Miyagoe-Suzuki Y & Takeda S. (2013). Activation of calcium signaling through Trpv1 by nNOS and peroxynitrite as a key trigger of skeletal muscle hypertrophy. *Nat Med* **19,** 101-106.

Jackman RW, Cornwell EW, Wu CL & Kandarian SC. (2013). Nuclear factor-kappaB signalling and transcriptional regulation in skeletal muscle atrophy. *Exp Physiol* **98,** 19-24.

Johnston AP, Baker J, De Lisio M & Parise G. (2011). Skeletal muscle myoblasts possess a stretch-responsive local angiotensin signalling system. *J Renin Angiotensin Aldosterone Syst* **12,** 75-84.

Kadoguchi T, Kinugawa S, Takada S, Fukushima A, Furihata T, Homma T, Masaki Y, Mizushima W, Nishikawa M, Takahashi M, Yokota T, Matsushima S, Okita K & Tsutsui H. (2015). Angiotensin II can directly induce mitochondrial dysfunction, decrease oxidative fibre number and induce atrophy in mouse hindlimb skeletal muscle. *Exp Physiol* **100,** 312-322.

Kandarian SC & Stevenson EJ. (2002). Molecular events in skeletal muscle during disuse atrophy. *Exerc Sport Sci Rev* **30,** 111-116.

Kelleher AR, Kimball SR, Dennis MD, Schilder RJ & Jefferson LS. (2013). The mTORC1 signaling repressors REDD1/2 are rapidly induced and activation of p70S6K1 by leucine is defective in skeletal muscle of an immobilized rat hindlimb. *Am J Physiol Endocrinol Metab* **304,** E229-236.

Koncarevic A, Jackman RW & Kandarian SC. (2007). The ubiquitin-protein ligase Nedd4 targets Notch1 in skeletal muscle and distinguishes the subset of atrophies caused by reduced muscle tension. *FASEB J* **21,** 427-437.

Kondo H, Miura M & Itokawa Y. (1991). Oxidative stress in skeletal muscle atrophied by immobilization. *Acta Physiol Scand* **142,** 527-528.

Kondo H, Nakagaki I, Sasaki S, Hori S & Itokawa Y. (1993). Mechanism of oxidative stress in skeletal muscle atrophied by immobilization. *Am J Physiol* **265,** E839-844.

Kwak YD, Wang B, Li JJ, Wang R, Deng Q, Diao S, Chen Y, Xu R, Masliah E, Xu H, Sung JJ & Liao FF. (2012). Upregulation of the E3 ligase NEDD4-1 by oxidative stress degrades IGF-1 receptor protein in neurodegeneration. *J Neurosci* **32,** 10971-10981.

Kwon OS, Smuder AJ, Wiggs MP, Hall SE, Sollanek KJ, Morton AB, Talbert EE, Toklu HZ, Tumer N & Powers SK. (2015). AT1 receptor blocker losartan protects against mechanical ventilation-induced diaphragmatic dysfunction. *J Appl Physiol (1985)* **119,** 1033-1041.

Latres E, Amini AR, Amini AA, Griffiths J, Martin FJ, Wei Y, Lin HC, Yancopoulos GD & Glass DJ. (2005). Insulin-like growth factor-1 (IGF-1) inversely regulates atrophy-induced genes via the phosphatidylinositol 3-kinase/Akt/mammalian target of rapamycin (PI3K/Akt/mTOR) pathway. *J Biol Chem* **280,** 2737-2744.

Lawler JM, Kunst M, Hord JM, Lee Y, Joshi K, Botchlett RE, Ramirez A & Martinez DA. (2014). EUK-134 ameliorates nNOSmu translocation and skeletal muscle fiber atrophy during short-term mechanical unloading. *Am J Physiol Regul Integr Comp Physiol* **306,** R470-482.

Lawler JM, Rodriguez DA & Hord JM. (2016). Mitochondria in the middle: Exercise preconditioning protection of striated muscle. *J Physiol*.

Lawler JM, Song W & Demaree SR. (2003). Hindlimb unloading increases oxidative stress and disrupts antioxidant capacity in skeletal muscle. *Free Radic Biol Med* **35,** 9-16.

Lecker SH, Jagoe RT, Gilbert A, Gomes M, Baracos V, Bailey J, Price SR, Mitch WE & Goldberg AL. (2004). Multiple types of skeletal muscle atrophy involve a common program of changes in gene expression. *FASEB J* **18,** 39-51.

Leri A, Claudio PP, Li Q, Wang X, Reiss K, Wang S, Malhotra A, Kajstura J & Anversa P. (1998). Stretch-mediated release of angiotensin II induces myocyte apoptosis by activating p53 that enhances the local renin-angiotensin system and decreases the Bcl-2-to-Bax protein ratio in the cell. *J Clin Invest* **101,** 1326-1342.

Llano-Diez M, Renaud G, Andersson M, Marrero HG, Cacciani N, Engquist H, Corpeno R, Artemenko K, Bergquist J & Larsson L. (2012). Mechanisms underlying ICU muscle wasting and effects of passive mechanical loading. *Crit Care* **16,** R209.

Lokireddy S, Wijesoma IW, Teng S, Bonala S, Gluckman PD, McFarlane C, Sharma M & Kambadur R. (2012). The ubiquitin ligase Mul1 induces mitophagy in skeletal muscle in response to muscle-wasting stimuli. *Cell Metab* **16,** 613-624.

Lomonosova YN, Kalamkarov GR, Bugrova AE, Shevchenko TF, Kartashkina NL, Lysenko EA, Shvets VI & Nemirovskaya TL. (2011). Protective effect of L-Arginine administration on proteins of unloaded m. soleus. *Biochemistry (Mosc)* **76,** 571-580.

Madrigal-Matute J, Fernandez-Laso V, Sastre C, Llamas-Granda P, Egido J, Martin-Ventura JL, Zalba G & Blanco-Colio LM. (2015). TWEAK/Fn14 interaction promotes oxidative stress through NADPH oxidase activation in macrophages. *Cardiovasc Res* **108,** 139-147.

Marimuthu K, Murton AJ & Greenhaff PL. (2011). Mechanisms regulating muscle mass during disuse atrophy and rehabilitation in humans. *J Appl Physiol (1985)* **110,** 555-560.

Marzec M, Eletto D & Argon Y. (2012). GRP94: An HSP90-like protein specialized for protein folding and quality control in the endoplasmic reticulum. *Biochim Biophys Acta* **1823,** 774-787.

Matuszczak Y, Arbogast S & Reid MB. (2004). Allopurinol mitigates muscle contractile dysfunction caused by hindlimb unloading in mice. *Aviat Space Environ Med* **75,** 581-588.

McClung JM, Van Gammeren D, Whidden MA, Falk DJ, Kavazis AN, Hudson MB, Gayan-Ramirez G, Decramer M, DeRuisseau KC & Powers SK. (2009). Apocynin attenuates diaphragm oxidative stress and protease activation during prolonged mechanical ventilation. *Crit Care Med* **37,** 1373-1379.

Merck. (2015). Cozaar (Losartan Potassium) Prescribing Information. www.merck.com/product/usa/pi_circulars/c/cozaar/cozaar_pi.pdf.

Milan G, Romanello V, Pescatore F, Armani A, Paik JH, Frasson L, Seydel A, Zhao J, Abraham R, Goldberg AL, Blaauw B, DePinho RA & Sandri M. (2015). Regulation of autophagy and the ubiquitin-proteasome system by the FoxO transcriptional network during muscle atrophy. *Nat Commun* **6,** 6670.

Min K, Smuder AJ, Kwon OS, Kavazis AN, Szeto HH & Powers SK. (2011). Mitochondrial-targeted antioxidants protect skeletal muscle against immobilization-induced muscle atrophy. *J Appl Physiol (1985)* **111,** 1459-1466.

Mittal A, Bhatnagar S, Kumar A, Lach-Trifilieff E, Wauters S, Li H, Makonchuk DY, Glass DJ & Kumar A. (2010). The TWEAK-Fn14 system is a critical regulator of denervation-induced skeletal muscle atrophy in mice. *J Cell Biol* **188,** 833-849.

Morales MG, Abrigo J, Acuna MJ, Santos RA, Bader M, Brandan E, Simon F, Olguin H, Cabrera D & Cabello-Verrugio C. (2016). Angiotensin-(1-7) attenuates disuse skeletal muscle atrophy in mice via its receptor, Mas. *Dis Model Mech* **9,** 441-449.

Mordenti J. (1986). Man versus beast: pharmacokinetic scaling in mammals. *J Pharm Sci* **75,** 1028-1040.

Munoz KA, Satarug S & Tischler ME. (1993). Time course of the response of myofibrillar and sarcoplasmic protein metabolism to unweighting of the soleus muscle. *Metabolism* **42,** 1006-1012.

Murata M, Kosaka R, Kurihara K, Yamashita S & Tachibana H. (2016). Delphinidin prevents disuse muscle atrophy and reduces stress-related gene expression. *Biosci Biotechnol Biochem***,** 1-5.

Nakao R, Hirasaka K, Goto J, Ishidoh K, Yamada C, Ohno A, Okumura Y, Nonaka I, Yasutomo K, Baldwin KM, Kominami E, Higashibata A, Nagano K, Tanaka K, Yasui N, Mills EM, Takeda S & Nikawa T. (2009). Ubiquitin ligase Cbl-b is a negative regulator for insulin-like growth factor 1 signaling during muscle atrophy caused by unloading. *Mol Cell Biol* **29,** 4798-4811.

Nguyen HX & Tidball JG. (2003). Expression of a muscle-specific, nitric oxide synthase transgene prevents muscle membrane injury and reduces muscle inflammation during modified muscle use in mice. *J Physiol* **550,** 347-356.

Nin N, Cassina A, Boggia J, Alfonso E, Botti H, Peluffo G, Trostchansky A, Batthyany C, Radi R, Rubbo H & Hurtado FJ. (2004). Septic diaphragmatic dysfunction is prevented by Mn(III)porphyrin therapy and inducible nitric oxide synthase inhibition. *Intensive Care Med* **30,** 2271-2278.

O'Loghlen A, Perez-Morgado MI, Salinas M & Martin ME. (2006). N-acetyl-cysteine abolishes hydrogen peroxide-induced modification of eukaryotic initiation factor 4F activity via distinct signalling pathways. *Cell Signal* **18,** 21-31.

Ohira Y, Jiang B, Roy RR, Oganov V, Ilyina-Kakueva E, Marini JF & Edgerton VR. (1992). Rat soleus muscle fiber responses to 14 days of spaceflight and hindlimb suspension. *J Appl Physiol (1985)* **73,** 51S-57S.

Pearson T, Kabayo T, Ng R, Chamberlain J, McArdle A & Jackson MJ. (2014). Skeletal muscle contractions induce acute changes in cytosolic superoxide, but slower responses in mitochondrial superoxide and cellular hydrogen peroxide. *PLoS One* **9,** e96378.

Phillips SM, Glover EI & Rennie MJ. (2009). Alterations of protein turnover underlying disuse atrophy in human skeletal muscle. *J Appl Physiol (1985)* **107,** 645-654.

Phillips SM & McGlory C. (2014). CrossTalk proposal: The dominant mechanism causing disuse muscle atrophy is decreased protein synthesis. *J Physiol* **592,** 5341-5343.

Pierre N, Barbe C, Gilson H, Deldicque L, Raymackers JM & Francaux M. (2014). Activation of ER stress by hydrogen peroxide in C2C12 myotubes. *Biochem Biophys Res Commun* **450,** 459-463.

Powers SK, Kavazis AN & McClung JM. (2007). Oxidative stress and disuse muscle atrophy. *J Appl Physiol (1985)* **102,** 2389-2397.

Quigley HA, Pitha IF, Welsbie DS, Nguyen C, Steinhart MR, Nguyen TD, Pease ME, Oglesby EN, Berlinicke CA, Mitchell KL, Kim J, Jefferys JJ & Kimball EC.

(2015). Losartan Treatment Protects Retinal Ganglion Cells and Alters Scleral Remodeling in Experimental Glaucoma. *PLoS One* **10,** e0141137.

Ramaswamy S, Nakamura N, Sansal I, Bergeron L & Sellers WR. (2002). A novel mechanism of gene regulation and tumor suppression by the transcription factor FKHR. *Cancer Cell* **2,** 81-91.

Reagan-Shaw S, Nihal M & Ahmad N. (2008). Dose translation from animal to human studies revisited. *FASEB J* **22,** 659-661.

Reid MB, Judge AR & Bodine SC. (2014). CrossTalk opposing view: The dominant mechanism causing disuse muscle atrophy is proteolysis. *J Physiol* **592,** 5345-5347.

Rudnick J, Puttmann B, Tesch PA, Alkner B, Schoser BG, Salanova M, Kirsch K, Gunga HC, Schiffl G, Luck G & Blottner D. (2004). Differential expression of nitric oxide synthases (NOS 1-3) in human skeletal muscle following exercise countermeasure during 12 weeks of bed rest. *FASEB J* **18,** 1228-1230.

Sacheck JM, Hyatt JP, Raffaello A, Jagoe RT, Roy RR, Edgerton VR, Lecker SH & Goldberg AL. (2007). Rapid disuse and denervation atrophy involve transcriptional changes similar to those of muscle wasting during systemic diseases. *FASEB J* **21,** 140-155.

Salazar JJ, Michele DE & Brooks SV. (2010). Inhibition of calpain prevents muscle weakness and disruption of sarcomere structure during hindlimb suspension. *J Appl Physiol (1985)* **108,** 120-127.

Sandona D, Desaphy JF, Camerino GM, Bianchini E, Ciciliot S, Danieli-Betto D, Dobrowolny G, Furlan S, Germinario E, Goto K, Gutsmann M, Kawano F, Nakai N, Ohira T, Ohno Y, Picard A, Salanova M, Schiffl G, Blottner D, Musaro A, Ohira Y, Betto R, Conte D & Schiaffino S. (2012). Adaptation of mouse skeletal muscle to long-term microgravity in the MDS mission. *PLoS One* **7,** e33232.

Sandri M, Sandri C, Gilbert A, Skurk C, Calabria E, Picard A, Walsh K, Schiaffino S, Lecker SH & Goldberg AL. (2004). Foxo transcription factors induce the atrophy-related ubiquitin ligase atrogin-1 and cause skeletal muscle atrophy. *Cell* **117,** 399-412.

Sartori R, Schirwis E, Blaauw B, Bortolanza S, Zhao J, Enzo E, Stantzou A, Mouisel E, Toniolo L, Ferry A, Stricker S, Goldberg AL, Dupont S, Piccolo S, Amthor H & Sandri M. (2013). BMP signaling controls muscle mass. *Nat Genet* **45,** 1309-1318.

Schiaffino S, Dyar KA, Ciciliot S, Blaauw B & Sandri M. (2013). Mechanisms regulating skeletal muscle growth and atrophy. *FEBS J* **280,** 4294-4314.

Schindler C, Bramlage P, Kirch W & Ferrario CM. (2007). Role of the vasodilator peptide angiotensin-(1-7) in cardiovascular drug therapy. *Vasc Health Risk Manag* **3,** 125-137.

Sellman JE, DeRuisseau KC, Betters JL, Lira VA, Soltow QA, Selsby JT & Criswell DS. (2006). In vivo inhibition of nitric oxide synthase impairs upregulation of contractile protein mRNA in overloaded plantaris muscle. *J Appl Physiol (1985)* **100,** 258-265.

Semprun-Prieto LC, Sukhanov S, Yoshida T, Rezk BM, Gonzalez-Villalobos RA, Vaughn C, Michael Tabony A & Delafontaine P. (2011). Angiotensin II induced catabolic effect and muscle atrophy are redox dependent. *Biochem Biophys Res Commun* **409,** 217-221.

Senf SM, Dodd SL, McClung JM & Judge AR. (2008). Hsp70 overexpression inhibits NF-kappaB and Foxo3a transcriptional activities and prevents skeletal muscle atrophy. *FASEB J* **22,** 3836-3845.

Shenton D, Smirnova JB, Selley JN, Carroll K, Hubbard SJ, Pavitt GD, Ashe MP & Grant CM. (2006). Global translational responses to oxidative stress impact upon multiple levels of protein synthesis. *J Biol Chem* **281,** 29011-29021.

Siu PM & Alway SE. (2005). Id2 and p53 participate in apoptosis during unloading-induced muscle atrophy. *Am J Physiol Cell Physiol* **288,** C1058-1073.

Smith LR & Barton ER. (2014). SMASH - semi-automatic muscle analysis using segmentation of histology: a MATLAB application. *Skelet Muscle* **4,** 21.

Smuder AJ, Hudson MB, Nelson WB, Kavazis AN & Powers SK. (2012). Nuclear factor-kappaB signaling contributes to mechanical ventilation-induced diaphragm weakness*. *Crit Care Med* **40,** 927-934.

Smuder AJ, Kavazis AN, Hudson MB, Nelson WB & Powers SK. (2010). Oxidation enhances myofibrillar protein degradation via calpain and caspase-3. *Free Radic Biol Med* **49,** 1152-1160.

Solomon V & Goldberg AL. (1996). Importance of the ATP-ubiquitin-proteasome pathway in the degradation of soluble and myofibrillar proteins in rabbit muscle extracts. *J Biol Chem* **271,** 26690-26697.

Song R, Peng W, Zhang Y, Lv F, Wu HK, Guo J, Cao Y, Pi Y, Zhang X, Jin L, Zhang M, Jiang P, Liu F, Meng S, Zhang X, Jiang P, Cao CM & Xiao RP. (2013). Central role of E3 ubiquitin ligase MG53 in insulin resistance and metabolic disorders. *Nature* **494,** 375-379.

Stitt TN, Drujan D, Clarke BA, Panaro F, Timofeyva Y, Kline WO, Gonzalez M, Yancopoulos GD & Glass DJ. (2004). The IGF-1/PI3K/Akt pathway prevents expression of muscle atrophy-induced ubiquitin ligases by inhibiting FOXO transcription factors. *Mol Cell* **14,** 395-403.

Sukhanov S, Semprun-Prieto L, Yoshida T, Michael Tabony A, Higashi Y, Galvez S & Delafontaine P. (2011). Angiotensin II, oxidative stress and skeletal muscle wasting. *Am J Med Sci* **342,** 143-147.

Sun QA, Hess DT, Nogueira L, Yong S, Bowles DE, Eu J, Laurita KR, Meissner G & Stamler JS. (2011). Oxygen-coupled redox regulation of the skeletal muscle ryanodine receptor-Ca2+ release channel by NADPH oxidase 4. *Proc Natl Acad Sci U S A* **108,** 16098-16103.

Suwa M, Nakano H, Radak Z & Kumagai S. (2015). Effects of Nitric Oxide Synthase Inhibition on Fiber-Type Composition, Mitochondrial Biogenesis, and SIRT1 Expression in Rat Skeletal Muscle. *J Sports Sci Med* **14,** 548-555.

Suzuki N, Motohashi N, Uezumi A, Fukada S, Yoshimura T, Itoyama Y, Aoki M, Miyagoe-Suzuki Y & Takeda S. (2007). NO production results in suspension-induced muscle atrophy through dislocation of neuronal NOS. *J Clin Invest* **117,** 2468-2476.

Tabony AM, Yoshida T, Galvez S, Higashi Y, Sukhanov S, Chandrasekar B, Mitch WE & Delafontaine P. (2011). Angiotensin II upregulates protein phosphatase

2Calpha and inhibits AMP-activated protein kinase signaling and energy balance leading to skeletal muscle wasting. *Hypertension* **58,** 643-649.

Tabony AM, Yoshida T, Sukhanov S & Delafontaine P. (2014). Protein phosphatase 2C-alpha knockdown reduces angiotensin II-mediated skeletal muscle wasting via restoration of mitochondrial recycling and function. *Skelet Muscle* **4,** 20.

Taillandier D, Aurousseau E, Meynial-Denis D, Bechet D, Ferrara M, Cottin P, Ducastaing A, Bigard X, Guezennec CY, Schmid HP & et al. (1996). Coordinate activation of lysosomal, Ca 2+-activated and ATP-ubiquitin-dependent proteinases in the unweighted rat soleus muscle. *Biochem J* **316 (Pt 1),** 65-72.

Talbert EE, Smuder AJ, Min K, Kwon OS & Powers SK. (2013a). Calpain and caspase-3 play required roles in immobilization-induced limb muscle atrophy. *J Appl Physiol (1985)* **114,** 1482-1489.

Talbert EE, Smuder AJ, Min K, Kwon OS, Szeto HH & Powers SK. (2013b). Immobilization-induced activation of key proteolytic systems in skeletal muscles is prevented by a mitochondria-targeted antioxidant. *J Appl Physiol (1985)* **115,** 529-538.

Tan PL, Shavlakadze T, Grounds MD & Arthur PG. (2015). Differential thiol oxidation of the signaling proteins Akt, PTEN or PP2A determines whether Akt phosphorylation is enhanced or inhibited by oxidative stress in C2C12 myotubes derived from skeletal muscle. *Int J Biochem Cell Biol* **62,** 72-79.

Tesch PA, von Walden F, Gustafsson T, Linnehan RM & Trappe TA. (2008). Skeletal muscle proteolysis in response to short-term unloading in humans. *J Appl Physiol (1985)* **105,** 902-906.

Thomason DB, Biggs RB & Booth FW. (1989). Protein metabolism and beta-myosin heavy-chain mRNA in unweighted soleus muscle. *Am J Physiol* **257,** R300-305.

Tidball JG, Lavergne E, Lau KS, Spencer MJ, Stull JT & Wehling M. (1998). Mechanical loading regulates NOS expression and activity in developing and adult skeletal muscle. *Am J Physiol* **275,** C260-266.

Urso ML, Scrimgeour AG, Chen YW, Thompson PD & Clarkson PM. (2006). Analysis of human skeletal muscle after 48 h immobilization reveals alterations in mRNA

and protein for extracellular matrix components. *J Appl Physiol (1985)* **101,** 1136-1148.

Vitadello M, Germinario E, Ravara B, Libera LD, Danieli-Betto D & Gorza L. (2014a). Curcumin counteracts loss of force and atrophy of hindlimb unloaded rat soleus by hampering neuronal nitric oxide synthase untethering from sarcolemma. *J Physiol* **592,** 2637-2652.

Vitadello M, Gherardini J & Gorza L. (2014b). The stress protein/chaperone Grp94 counteracts muscle disuse atrophy by stabilizing subsarcolemmal neuronal nitric oxide synthase. *Antioxid Redox Signal* **20,** 2479-2496.

Waddell DS, Baehr LM, van den Brandt J, Johnsen SA, Reichardt HM, Furlow JD & Bodine SC. (2008). The glucocorticoid receptor and FOXO1 synergistically activate the skeletal muscle atrophy-associated MuRF1 gene. *Am J Physiol Endocrinol Metab* **295,** E785-797.

Watson ML, Baehr LM, Reichardt HM, Tuckermann JP, Bodine SC & Furlow JD. (2012). A cell-autonomous role for the glucocorticoid receptor in skeletal muscle atrophy induced by systemic glucocorticoid exposure. *Am J Physiol Endocrinol Metab* **302,** E1210-1220.

Wei Y, Sowers JR, Nistala R, Gong H, Uptergrove GM, Clark SE, Morris EM, Szary N, Manrique C & Stump CS. (2006). Angiotensin II-induced NADPH oxidase activation impairs insulin signaling in skeletal muscle cells. *J Biol Chem* **281,** 35137-35146.

Whidden MA, McClung JM, Falk DJ, Hudson MB, Smuder AJ, Nelson WB & Powers SK. (2009). Xanthine oxidase contributes to mechanical ventilation-induced diaphragmatic oxidative stress and contractile dysfunction. *J Appl Physiol (1985)* **106,** 385-394.

Whitehead NP, Yeung EW, Froehner SC & Allen DG. (2010). Skeletal muscle NADPH oxidase is increased and triggers stretch-induced damage in the mdx mouse. *PLoS One* **5,** e15354.

Wittwer M, Fluck M, Hoppeler H, Muller S, Desplanches D & Billeter R. (2002). Prolonged unloading of rat soleus muscle causes distinct adaptations of the gene profile. *FASEB J* **16,** 884-886.

Wu CL, Kandarian SC & Jackman RW. (2011). Identification of genes that elicit disuse muscle atrophy via the transcription factors p50 and Bcl-3. *PLoS One* **6,** e16171.

Xiao L, Hu SQ, Wang LY, Liu JX & Li XY. (2015). Losartan improves the distribution and efficacy of doxorubicin in CT26 tumor. *Eur Rev Med Pharmacol Sci* **19,** 3763-3769.

You JS, Park MN, Song W & Lee YS. (2010). Dietary fish oil alleviates soleus atrophy during immobilization in association with Akt signaling to p70s6k and E3 ubiquitin ligases in rats. *Appl Physiol Nutr Metab* **35,** 310-318.

Zhang L, Kimball SR, Jefferson LS & Shenberger JS. (2009). Hydrogen peroxide impairs insulin-stimulated assembly of mTORC1. *Free Radic Biol Med* **46,** 1500-1509.

Zhao W, Swanson SA, Ye J, Li X, Shelton JM, Zhang W & Thomas GD. (2006). Reactive oxygen species impair sympathetic vasoregulation in skeletal muscle in angiotensin II-dependent hypertension. *Hypertension* **48,** 637-643.

Zhu B, Sun Y, Sievers RE, Browne AE, Pulukurthy S, Sudhir K, Lee RJ, Chou TM, Chatterjee K & Parmley WW. (2000). Comparative effects of pretreatment with captopril and losartan on cardiovascular protection in a rat model of ischemia-reperfusion. *J Am Coll Cardiol* **35,** 787-795.

Zhu BQ, Sievers RE, Browne AE, Lee RJ, Chatterjee K, Grossman W, Karliner JS & Parmley WW. (2003). Comparative effects of aspirin with ACE inhibitor or angiotensin receptor blocker on myocardial infarction and vascular function. *J Renin Angiotensin Aldosterone Syst* **4,** 31-37.

Zou Y, Akazawa H, Qin Y, Sano M, Takano H, Minamino T, Makita N, Iwanaga K, Zhu W, Kudoh S, Toko H, Tamura K, Kihara M, Nagai T, Fukamizu A, Umemura S, Iiri T, Fujita T & Komuro I. (2004). Mechanical stress activates angiotensin II type 1 receptor without the involvement of angiotensin II. *Nat Cell Biol* **6,** 499-506.

APPENDIX

Justification for the Dosage of Losartan

In the present study, rats that received losartan were administered a dose of 30-40 mg/kg/day via intraperitoneal (i.p.) injection. The rationale for using this concentration of losartan is based on the dose used in previous myopathy studies (Habashi *et al.*, 2006; Cohn *et al.*, 2007; Burks *et al.*, 2011), which used dosages that achieved a 10 – 20% decrease in heart rate and blood pressure, measurements that are deemed desirable in humans (Habashi *et al.*, 2006). When normalized to standard body surface area (BSA), 30-40 mg/kg dosage for a 300 gram rat translates to an approximate dose of 6-8 mg/kg/day in humans (Reagan-Shaw *et al.*, 2008).

Due to differences in drug absorption, metabolism, and elimination, larger doses are required in order to achieve similar pharmacological effects to those that are observed in humans (Mordenti, 1986). Several previously published studies have administered 40 mg/kg/day of losartan in adult rats without any toxic effects reported (Zhu *et al.*, 2000; Zhu *et al.*, 2003; Goncalves *et al.*, 2005; Quigley *et al.*, 2015). Additionally, 30-40 mg/kg dosage is far below the 2000 mg/kg dose that led to significant lethality in adult rats (Merck, 2015). Therefore, the dosage of losartan used in the present study is a non-toxic and translatable amount.

Table A1. Primary Antibodies

Antibody	Dilution	Company	Catalog #	Experiment
GAPDH	1:10,000	EMD/Millipore	MAB374	Western Blotting
Na+/K+ ATPase	1:1,000	Cell Signaling Technology	05-369	Western Blotting
Histone H3	1:1,000	Cell Signaling Technology	9715	Western Blotting
gp91phox	1:1,000	BD Biosciences	611415	Western Blotting
p67phox	1:2,500	BD Biosciences	610913	Western Blotting
p47phox	1:750	BD Biosciences	610355	Western Blotting
Rac-1	1:500	EMD/Millipore	07-1464	Western Blotting
nNOS	1:750	Life Technologies / Thermo Fisher Scientific	61-700	Western Blotting
FoxO3a	1:750	Cell Signaling Technology	12829	Western Blotting
p53	1:750	Cell Signaling Technology	2527	Western Blotting

Table A1. Primary Antibodies (continued)

Antibody	Dilution	Company	Catalog #	Experiment
Dystrophin	1:100	Santa Cruz Biotechnology	sc-15376	Immunofluorescence
Slow Skeletal Myosin	1:250	Abcam	ab11083	Immunofluorescence
Fast Skeletal Myosin	1:250	Abcam	ab51263	Immunofluorescence
β-Sarcoglycan	1:200	Abcam	ab55683	Immunofluorescence
nNOS	1:100	Cayman Chemical	160870	Immunofluorescence
FOXO3a (FKHRL1)	1:50	Sigma	SAB3500508	Immunofluorescence

Table A2. Secondary Antibodies

Antibody	Dilution	Company	Catalog #	Experiment
Goat Anti-Rabbit IgG-HRP	1:5,000	Santa Cruz Biotechnology	sc-2004	Western Blotting
Goat Anti-Mouse IgG-HRP	1:5,000	Santa Cruz Biotechnology	sc-2005	Western Blotting
Goat Anti-Rabbit IgG (H+L) Secondary Antibody, Alexa Fluor 594 conjugate	1:200	Life Technologies / Thermo Fisher Scientific	A-11037	Immunofluorescence
Goat-Anti-Mouse IgG (H+L) Secondary Antibody, Alexa Fluor 594 conjugate	1:200	Life Technologies / Thermo Fisher Scientific	A-11005	Immunofluorescence

Table A2. Secondary Antibodies (continued)

Antibody	Dilution	Company	Catalog #	Experiment
Goat Anti-Rabbit IgG (H+L) Secondary Antibody, Alexa Fluor 488 conjugate	1:200	Life Technologies / Thermo Fisher Scientific	A-11008	Immunofluorescence
Goat-Anti-Mouse IgG (H+L) Secondary Antibody, Alexa Fluor 488 conjugate	1:200	Life Technologies / Thermo Fisher Scientific	A-11001	Immunofluorescence

Table A3. Injectable Reagents

Reagent	Company	Catalog #
Ketamine	Henry Schein	045822
Xylazine	Lloyd (from Henry Schein)	033198
Somnasol – Euthanasia III Solution (Pentobarbital Sodium)	Henry Schein	024352
Losartan (potassium salt)	Cayman Chemical	10006594
0.9% Sodium Chloride (Saline) Injection, USP	Hospira	0409-7984

Table A4. Buffer Reagents

Reagent	Company	Catalog #
Tris-HCl (Trizma hydrochloride)	Sigma-Aldrich	T5941
NaCl (sodium chloride)	Sigma-Aldrich	S9625
EDTA (ethylenediaminetetraacetic acid)	Sigma-Aldrich	ED
EGTA (ethylene glycol-bis(2-aminoethylether)-*N,N,N',N'*-tetraacetic acid)	Sigma-Aldrich	E3889
Sucrose	Sigma-Aldrich	S-7903
$MgCl_2$ (magnesium chloride hexahydrate)	Sigma-Aldrich	M-2670
HEPES	Sigma-Aldrich	H4034
Glycerol	Sigma-Aldrich	G5516
Triton X-100	MP Biomedicals	194854
Tween-20	Thermo Fisher Scientific	P1379
NBT (nitrotetrazolium blue chloride)	Sigma-Aldrich	N6639
Beta-NADPH (β-nicotinamide adenine dinucleotide 2'-phosphate reduced tetrasodium salt hydrate)	Sigma-Aldrich	N7505
Protease Inhibitor Cocktail Mini Tablets; EDTA-free	Thermo Fisher Scientific	88666

Table A5. Western Blotting Reagents

Reagent	Company	Catalog #
Non-fat dry milk	Carnation	
Ponceau S	Sigma-Aldrich	P3504
Bradford Dye Reagent Concentrate	Bio-Rad	500-0006
Super Signal West Dura Extended Duration Substrate	Thermo Fisher Scientific	34076
Precision Plus Protein Kaleidoscope Standards	Bio-Rad	161-0375

Table A6. Histochemistry Reagents

Reagent	Company	Catalog #
O.C.T. (Optimal Cutting Temperature) Compound	Fisher HealthCare	4585
Hematoxylin	VWR	95057-844
Eosin	VWR	95057-846
Wheat Germ Agglutinin, Alexa Fluor 555 Conjugate	Life Technologies / Thermo Fisher Scientific	W32464
DAPI (4',6-Diamidino-2-Phenylindole, Dihydrochloride)	Life Technologies / Thermo Fisher Scientific	D1306
Normal Goat Serum (10%) Blocking Solution	Life Technologies / Thermo Fisher Scientific	50062Z
VectaMount Permanent Mounting Medium	Vector Laboratories	H-5000
ProLong Gold Anti-Fade Mountant	Life Technologies / Thermo Fisher Scientific	P36930

Table A7. Reactive Oxygen Species (ROS) Detection and Inhibition Reagents

Reagent	Company	Catalog #
Dihydroethidium (DHE)	Life Technologies / Thermo Fisher Scientific	D1168
Lucigenin	Cayman Chemical	14872
EUK 134	Cayman Chemical	10006329
Diphenyleneiodonium Chloride (DPI)	Sigma-Aldrich	D2926
gp91dstat	Bio-synthesis, Inc.	Custom: [NH2]YGRKKRRQRRRCSTRIRRQL[CONH2]

NOMENCLATURE

4E-BP1	4E-Binding Protein 1
ACE	Angiotensin Converting Enzyme
ALS	Amyotrophic Lateral Sclerosis
AngII	Angiotensin II
Ang-1(1-7)	Angiotensin-1(1-7)
AT1R	Angiotensin II Type 1 Receptor
ATF4	Activating Transcription Factor 4
BSA	Body Surface Area
COPD	Chronic Obstructive Pulmonary Disease
CSA	Cross-Sectional Area
CSC	Cross-Sectional Circumference
DETC	Diethyl-Dithiocarbamate
DGC	Dystrophin Glycoprotein Complex
DHE	Dihydroethidium
DPI	Diphenyleneiodonium
EUK134	Eukaryion 134
Fn14	Fibroblast Growth Factor-Inducible 14
FoxO	Forkhead Members of the Class O
GR	Glucocorticoid Receptor
Grp94	Glucose-Regulated Protein 94

HSP	Heat Shock Protein
IGF-1	Insulin-Like Growth Factor-1
IGFR	Insulin-Like Growth Factor Receptor
IκB	Inhibitor of Kappa B
iNOS	Inducible Nitric Oxide Synthase
i.p.	Intraperitoneal
IRS-1	Insulin Receptor Substrate-1
MAFbx	Muscle Atrophy F-Box
MG53	Mitsugumin 53
MGD	*N*-Methyl-*D*-Glucamine-Dithiocarbamate
MHC	Myosin Heavy Chain
mTORC1	Mammalian Target of Rapamycin Complex 1
Mul1	Mitochondrial E3 ubiquitin ligase 1
MuRF1	Muscle Specific RING Finger Protein 1
MUSA1	Muscle Ubiquitin Ligase of SCF Complex in Atrophy - 1
NADPH	Nictotinamide Adenine Dinucleotide Phosphate
Nox	NADPH Oxidase
NFκB	Nuclear Factor Kappa B
nNOS	Neuornal Nitric Oxide Synthase
•NO	Nitric Oxide
PI3K	Phosphatidylinositol-3 Kinase
RAS	Renin-Angiotensin System

ROS	Reactive Oxygen Species
SEM	Standard Error Mean
TRIM72	Tripartite Motif 72
ULLS	Unilateral Lower Limb Suspension
UPP	Ubiquitin Proteasome Pathway
WGA	Wheat Germ Agglutinin
XO	Xanthine Oxidase